Designing Atomic Interfaces in Chalcogenides for Boosting Photocatalysis

Mengmeng Ma, Huaping Zhao, Zhijie Wang,* and Yong Lei*

A deeper understanding of interfaces comes after the rapid development of nano-hybrids. Atomic interfaces with atomic-level thickness, intimate bonds, inferior charge-transport resistance, and robust stability have received escalating interest in the field of photocatalysis. Taking into account the fact that the carrier dynamics and spectrum response of candidate photocatalysts like chalcogenides remain suffering, sustained efforts are devoted. Hybridization, which is accompanied by interface designing, behaves as a supportive strategy to enlarge the photocatalytic output. Hence, the comprehensive survey for recent empirical studies on atomic interfaces in chalcogenides is highly desirable. Precisely, the fundamental of atomic interfaces, the devised approaches to design atomic interfaces in chalcogenides and their feasible roles for maneuvering photocatalysis, and the auxiliary advanced characterization are enumerated and summarized. The multifarious interaction of structure, chemical environment, optical and electric properties, and photocatalytic performance in chalcogenides with atomic interfaces is highlighted. Meanwhile, perspectives of atomic interfaces benefiting photocatalysis are given with a summary, and outlooks related to controllable architecture, nucleation mechanism, calculation, and the correlation between atomic interfaces and amended photocatalysis are presented discreetly. Herein, the review is meant to provide the first systematic account of designing atomic interfaces in chalcogenides served for ultimate photocatalytic applications.

1. Introduction

Interface has long been a critical issue in the fields of solar cells,[1] light-emitting devices,[2] solid-state batteries,[3] photocatalysis,[4] and any other involving multiphase systems.[5] Early perceptions of interfaces seem to be limited to differences in phases. With the rapid development of nanoscience, the definition of interface begins to develop from macroscale to micro/nanoscale perspective.[6] From the shape type (pointed, linear, and planar) to the comprehensive properties of thickness, composition, and stability, interface is gradually being deeper understood.[7] No exception, the characteristics of solid–solid and solid–liquid interfaces are absolutely crucial for energy conversion in photocatalysis,[8] where surface redox reactions are economically driven by photogenerated carriers.

Photocatalysis has emerged as a powerful platform for solar energy harvesting, conversion, and storage.[9] In this way, the far-flung but intermittent solar energy has a sustainable window to output. During typical photocatalysis progress, semiconductors with suitable band structures serve as light absorbers and then convert solar energy into energy carried in charge carriers after complicated light–matter interactions.[10] Ultimate deployments, such as carbon dioxide (CO_2) reduction, generation of clean hydrogen (H_2) energy, pollutant degradation, disinfection, nitrogen fixation, and artificial photosynthesis, are expected to bring feasible solutions to the current-deteriorating global environment and energy apprehensions.[11] Obviously, the utilization of a mono bare component is restricted since it is so far impossible to integrate all the favorable factors required for photocatalysis. Long-term exploration has witnessed hybridization standing out among enlightened strategies aimed at broadening light absorption, improving charge separation efficiency,

M. Ma, Z. Wang
Key Laboratory of Semiconductor Materials Science
Beijing Key Laboratory of Low Dimensional Semiconductor Materials and Devices
Institute of Semiconductors
Chinese Academy of Sciences
Beijing 100083, China
E-mail: wangzj@semi.ac.cn

M. Ma, Z. Wang
Center of Materials Science and Optoelectronics Engineering
University of Chinese Academy of Sciences
Beijing 100049, China

H. Zhao, Y. Lei
Fachgebiet Angewandte Nanophysik
Institut für Physik & IMN MacroNano
Technische Universität Ilmenau
98693 Ilmenau, Germany
E-mail: yong.lei@tu-ilmenau.de

ADVANCED
SCIENCE NEWS
www.advancedsciencenews.com

Solar
RRL

www.solar-rrl.com

extending the utilization of charge carriers, and enriching active sites.[12] Hybridization brings not only integrated superiorities but also more or less inevitable interfaces. There is a growing body of literature that recognizes the importance of interface in photocatalysis.[13] When unfavorable, the interface acts as a barrier or bottleneck for charge and energy transport or as a carrier recombination center.[14] Conversely, a decent interface ensures efficient charge separation and weakened activation resistance. What plays a decisive role is the nature of the interface, especially whether the interfacial contact is tight and stable. Atomic interfaces can broadly be defined as interfaces with ultrathin thickness, atomic bonding between different phases, small contact resistance, and sound stability, which attract considerable research attention due to their essential role in low resistance in charge flow and intense charge distribution.

Modifying an excellent interface with a compacted substrate semiconductor would be the icing on the cake. Chalcogenides (sulfides, selenides, tellurides) behave as an intriguing class of high-profile photocatalysts by virtue of their abundant element composition, tunable optical properties, fascinating structural diversity, and available carrier mobility.[15] On the one hand, Cd or Zn (II B metals)–based chalcogenides possess considerable competitiveness as dominant light absorbers for photocatalysis. CdS and ZnS and their ternary (II–III–VI, II–IV–VI) or even multinary derivatives have been showing popularity for a long time.[16] A wide range of nontoxic metal chalcogenides photocatalysts (such as Cu-based Cu–S, Cu–III–VI, Cu–IV–VI, Cu–III–II–VI, Cu–II–IV–VI, and other I–V–VI) are now extensive available after decades of continuous research.[17] Intelligent design of components and morphologies pave a broader way for the utilization of these types of chalcogenides. However, certain limitations like charge recombination, monotonous light response, and limited active sites still demand ways to relieve them. On the other hand, 2D few-layered transition-metal dichalcogenides (TMDs) also unleash their captivating charm as electrocatalysis and co-catalysis.[18] Most predominantly, MoS_2 and $MoSe_2$ are among the most widely employed materials for hydrogen evolution due to their advantageous electrical conductivity and abundant active sites, and their properties have been thoroughly investigated.[19] Their various loading methods urgently need to be sorted out for further guidance.[19b] In pursuit of decent carrier dynamics and comprehensive photocatalytic output, countless kinds of potent hybrids and rational designs of atomic interfaces based on chalcogenides have attracted substantial attention from researchers.[20] A systematic arrangement of atomic interfaces rudiments of chalcogenides for diverse photocatalytic progress, including but not limited to H_2 evolution, CO_2 reduction, pollutant treatment, and photochemical synthesis, could provide vital advancement and insight into this field. However, a search of the literature revealed few reviews of interfaces in chalcogenides focus on the field of photocatalysis.

Hence, of particular concern in this review article is atomic interfaces in chalcogenides served for boosting photocatalysis. We start by elaborating on the fundamental of atomic interfaces and their significance in properties regulation in Section 2. Section 3 outlines strategies to architect atomic interfaces in chalcogenides, including self-assembly, defect-induced chemical bonds, cation exchange, and slow epitaxy. We then highlight the complex interaction between structure, chemical environment, optical and electric properties, and photocatalytic output in chalcogenides with atomic interfaces by reviewing the current advances by category and identifying the main benefits in Section 4. Section 5 presents the current advanced characterizations served for atomic interfaces. In addition, a brief summary and a discussion on the future development of atomic interfaces in chalcogenides involved in photocatalysis are proposed in Section 6. Through critical thinking on rational designing atomic interfaces in chalcogenides photocatalysts, our review aims to consolidate and proceed the profound insight into the feasible behaviors of atomic interfaces in the photocatalysis process.

2. The Fundamental of Atomic Interfaces

Existing in various forms, interfaces can be categorized contingent on how the different phases behave from a macro perspective. Specifically, to the interfaces of the photocatalyst hybrid, a multiphase suspended particle system, our review focuses more attention on and only discusses the solid–solid interfaces of heterogeneous photocatalyst powders. From the microscopic perspective, interfaces appear where the periodic arrangement of atoms is broken on a relatively large scale. Distinguished from physical mixing, interfaces of different phases which we care about are constructed usually via some local weak or strong force. Previous interest concentrates on the dimensional difference of the interfaces, such as point, linear, and planar contact. Luo and coworkers detailed these interfaces in their review.[7] Nevertheless, this difference in dimension or structural design from a morphology perspective is merely one of the factors of interface properties. Component, morphology, chemical environment, and stability consist of four basic building blocks of a termed interface (**Figure 1**a). Atomic interfaces highlight diverse components (since the interface is always the extension and diffusion region of adjacent phases), irregular morphologies with ultrathin thickness, complex chemical environment and surroundings, and robust stability thanks to atomic intense bonds. These vital criteria endow atomic interfaces with a small interfacial contact resistance and compelling thorough properties.

Solid-phase chalcogenides feature significant covalent bonds, including VI–VI bonds in some structures. For this reason, chalcogenides often display 2D layered structures or other low-dimensional structures in the form of nonionic groups. VI atoms arrangement makes up half of the framework of chalcogenides; therefore, the characteristics of VI elements need to be fully considered in the construction of the atomic interface of chalcogenides. 1) Often the ways to construct chalcogenides hybrids are via electrostatic attractions and van der Waals forces, which may be deemed weak but sufficient enough to develop atomic-level interfaces. Atomic interfaces could be architected via a self-assembly approach driven by electrostatic interaction or weak van der Waals forces (Figure 1b,c). The electrostatic interaction is mainly responsible for the attraction between charged materials. The weak van der Waals force is widely considered a contributing force but not the dominant force in the interfacial region.[21] 2) Much stronger chemical bonds and shared lattices are increasingly becoming the hinges of building atomic interfaces. Defects or modulation of growth rates in situ benefit

2300025 (2 of 25)
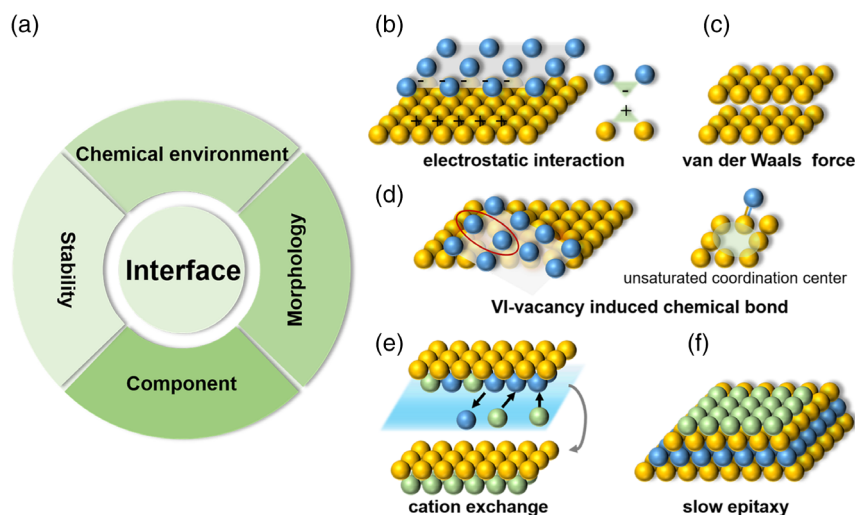
Figure 1. a) The building blocks of the interface. b–f) The simplified schematic illustration of the four approaches to design atomic interfaces in chalcogenides hybrids: b) Self-assembly approaches via electrostatic attraction or c) weak van der Waals force, d) VI-vacancies induced chemical bonds, e) cation exchange method, and f) slow epitaxy.

inducing these supportive intense bonds. Defects are usually manufactured with the hosts' geometric structure amended and the chemical environment adjusted by direct introduction or posttreatment,[22] resulting the changes in donor densities as well as optical and electronic properties.[23] Moreover, defects are able to sensitively regulate the host lattice coordination numbers, which may facilitate the interfacial chemical bonds. Generally, VI vacancy defects in chalcogenides are widely formed and thus the left coordinative unsaturated VI atoms could serve as an anchoring bridge for chemical bonds (Figure 1d). The shared lattice contains the extension of partial atoms arrangement and the extension of the lattice parameters, and we distinguish 3) the former as the cation exchange and 4) the latter as slow epitaxy (Figure 1e,f). These four devised approaches to design atomic interfaces in chalcogenides hybrid will be discussed in detail later in part 3 using specific pioneering efforts, respectively.

In the current extensive recognition, an available photocatalytic device for practical photocatalytic applications is required to possess the merit of wide-spectrum response, efficient charge excitation and separation, high utilization of surface carriers, and robust photochemical stability.[10,24] For a well-defined heterointerface hybrid, the aforementioned requirements have a chance to be integrated.[25] Current interfaces existing in photocatalytic devices are configured to be accompanied by hybridization for sufficient spectral utilization, charge separation, and enrichment of active sites.[12c,26] To achieve established enhancement, the primary consideration and principle for designing atomic interfaces are energy band alignment and the resulting kinetic preponderance. As schematically illustrated in **Figure 2**a–d, current feasible designed atomic interfaces in chalcogenides-based photocatalysts included a Z-scheme interface (similar S-scheme), type II interface, semiconductor–metal interface, and semiconductor–plasmonic metal interface. The essential band alignment, light absorption, charge flow, and the underlying advantages for charge segregation and sufficient carrier utilization are all contained in this illustration. The Z-scheme interface features the ability to maintain both strong reducing and oxidizing capabilities.

Chalcogenides with high-conduction band levels could keep their robust reduction propulsion and serve for a series of surface reactions driven by electrons; while some chalcogenides with weak reducing potential scarify their photoinduced electrons to recombine with holes in adjacent semiconductors and enhance the overall charge separation in the hybrids. Type II interface guarantees a kinetically favorable charge flow with fewer requirements for energy band but a relative alignment. Two CdS-based interfaces reported previously are taken as representatives and presented later in the schematical illustration in Figure 2a,b to supplementarily describe the characters of the Z-scheme interface and type II interface. It exhibits a totally different interfacial charge-transfer route and different catalytic site between $ZnIn_2S_4$/CdS Z-scheme interface and CuS/CdS type II interface. CdS generates electrons to recombine with the holes in $ZnIn_2S_4$ and $ZnIn_2S_4$ obtains improved charge separation and reduction ability at the Z-scheme hybrid;[27] while CdS accepts the electrons from CuS and serves as a connection to the terminal reduction site at the type II interface.[28] Experience has shown that type I heterojunction can play a similar role in charge separation of the conduction band in the presence of the sacrificial agent. We here distinguish two kinds of semiconductor–metal interface by the flow direction of photogenerated electrons. One is that the metal serves as the acceptor of electrons generated by chalcogenides and at the same time as the catalytic site of the reduction reaction; the other is the interface between chalcogenides and noble metals, which possess localized surface plasmon resonance (LSPR) effect. In the latter case, hot electrons generated by the photoexcited noble metals are injected into the conduction band of the neighboring semiconductors. As an example, CuS/Au interface (listed in Figure 2c,d) was revealed to display two electron-transfer directions, one is CuS to Au in a normal semimetal interface,[29] and the other is plasmonic Au-injecting hot electrons to CuS across the semi-plasmonic metal interface.[30] The reason for this difference is whether the LSPR effect of the plasmonic metal is excited, which depends on whether the incident light matches the response range of the plasmonic metals.
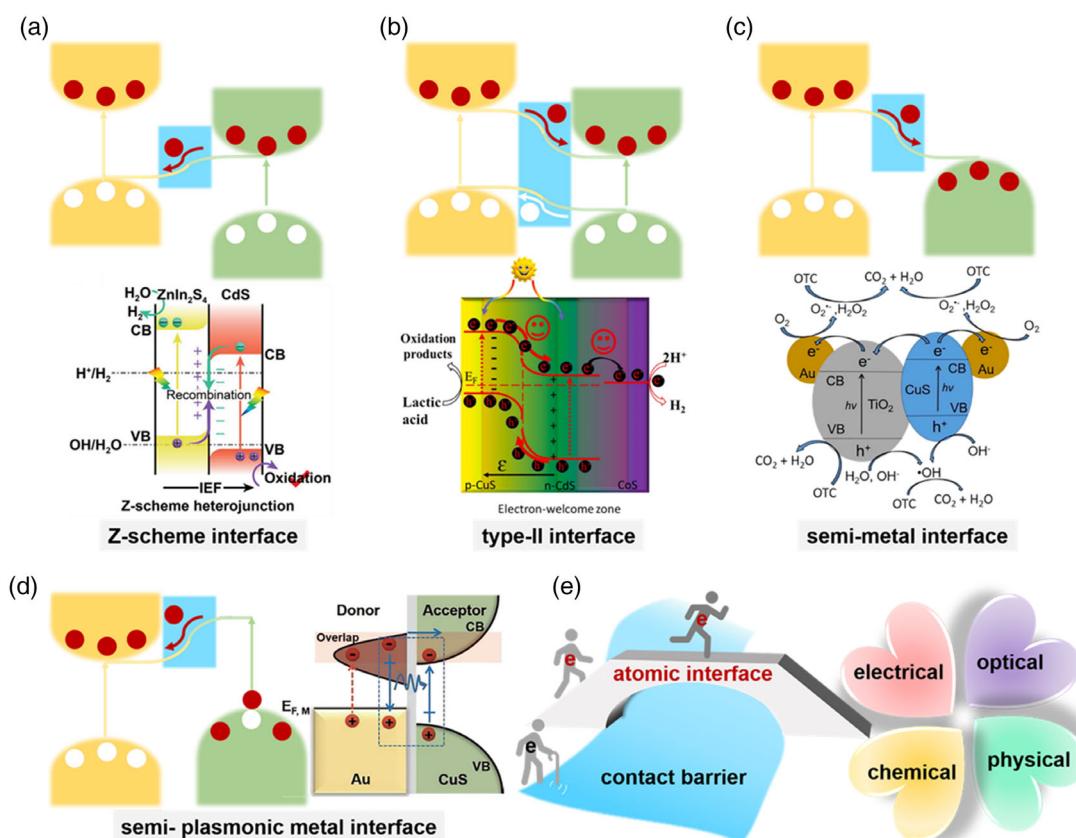
Figure 2. Schematic illustration of feasible designing atomic interfaces and the additional corresponding experimental models in chalcogenides-based photocatalysts from the perspective of energy band structure: a) Z-scheme interface, the picture below is a selected experimental model to additionally explain Z-scheme interface. Reproduced with permission.[27] Copyright 2022, Wiley-VCH. b) Type II interface, the picture provided is a selected experimental case to additionally explain the type II interface. Reproduced with permission.[28] Copyright 2022, Elsevier. c) Semiconductor–metal interface, the picture provided is a picked experimental model to help explain the semiconductor–metal interface. Reproduced with permission.[29] Copyright 2016, Elsevier. d) Semiconductor–plasmonic metal interface, the right image is attached to assist explain the semiconductor–plasmonic metal interface. Reproduced with permission.[30] Copyright 2022, Springer Nature. e) The access to the regulation of electrical, optical, physical, and chemical properties in photocatalyst hybrids via designing atomic interface "bridges."

Notably, the band alignment at the interface provides the theoretical fundamental for boosting photocatalysis from the aspects of light utilization, charge separation, and active sites. No matter which kind of interface is built, more importantly, the charge flow as expected in real situations is the key factor to breaking through the contact barrier. The commonly constructed solid–solid interface shows obvious interfacial resistance and bottleneck for charge-carrier migration. At this time, atomic interfaces serve as a sound bridge to overcome this contact barrier and transport the charge carriers easily. The smooth carrier flow across atomic interfaces preserves the subsequent access to the modulated and amended multi-property, including electrical, optical, chemical, and physical properties (Figure 2e), which is durably demanded by the well-established photocatalytic processes. It calls for in-depth insight and a comprehensive understanding of the interfaces to access the intrinsic and outer rational design of these properties. Therefore, developing insights into the formation and underlying enhancement mechanism of atomic interfaces is of critical significance for chalcogenides hybrids with highly upgraded photocatalysis performance. The ultrathin thickness, small contact resistance, and attractive chemical environment hold underlying effects for harnessing atomic interfaces as vital factors in chalcogenides-based photocatalytic applications. The excitation of charge carriers, recombination of excitons, and activation of catalytic reactions can be modulated by atomic-scale interfacial modifications. Therefore, there will be a significant improvement in the overall properties of the hybrid by synergistic effects, often occurring as a result of atomic interfaces. Hence, Chapter 4 moves on to discuss the roles of atomic interfaces in chalcogenides in detail.

3. The Devised Approaches for Atomic Interfaces of Chalcogenides

The properties of interfaces are mainly governed by the spatial distribution of atoms and intense bonding; thus, learning how to control both features is of utmost significance to optimize interfaces for the desired photocatalysis capability. The controllable construction of interfaces desires an appropriate formation method, while the characteristics of chalcogenides need to be taken into full consideration in the rational strategies to form

atomic interfaces in chalcogenides-based photocatalysts. In this review, the reported atomic interfaces are divided into four categories according to different bonds, including self-assemble atomic interfaces by weak interaction (electrostatic attraction and van der Waals force), atomic interfaces with intense metal–nonmetal bonds induced by VI defects, atomic interfaces established by in situ cation exchange, and epitaxy atomic interfaces. **Table 1** enumerates some typical cases describing auxiliary the diverse approaches to fabricating atomic interfaces in chalcogenide-based hybrids.

3.1. Self-Assembled Interfaces

Self-assembly behaves as a process that the basic structural units, like nanomaterials, molecules, or substances at the scale of micrometers or larger, form ordered and stable structures spontaneously. This process relies on the non-covalent bond. Nano-heterojunctions that we here discuss are synthesized by simplistic electrostatic-driven or weak-force self-assembling tactics. Electrostatic attraction is a property reflecting on the surface of nanomaterials, while interfaces are the results of infinitely close surfaces. Such interfaces also constitute atomic interfaces since they retain the positive and negative surface charges of the materials that attract each other. Weak van der Waals interactions are unique to 2D materials with large specific surface areas. From a summative point of view, slow interfacial nucleation or a high temperature and long reaction condition are also favorable factors for the formation of atomic-level interfaces.

A kind of 1D CdS nanorods/Ti_3C_2 Mxene nanosheet architecture was fabricated for enhanced photocatalytic H_2 evolution.[31] Benefiting from the atomic thickness of 2D Ti_3C_2 Mxene nanosheets, the subsequent generation of CdS nanorods was in an in situ assembling manner during the solvothermal progress, and CdS anchored on delaminated ultrathin Ti_3C_2 with a strong electrostatically driven interfacial coupling. The specific interface between CdS and Mxene was characterized as a Schottky heterojunction, which is devoted to accelerated charge separation. The atomic interface with intimate contact unveils the origin of the sevenfold advancement in hydrogen evolution reaction (HER) performance than pristine CdS. This work provides a reference for the merit of the atomic Schottky-type interface for boosted photocatalysis. The self-assembly during one-pot hydrothermal was also used to fabricate the interface of CeO_x-S/$ZnIn_2S_4$ catalysts.[32] Surface vulcanization, on the one hand, increases the CeO_2 surface-negative charge density; therefore, CeO_x–S is more closely anchored to the $ZnIn_2S_4$ surface. On the other hand, the engendered oxygen vacancies are of great significance to CO_2 photocatalytic reduction. Similarly, $ZnIn_2S_4$ was assembled on the surface of hollow tubular In_2O_3 both inner and outer during a hydrothermal process (shown in **Figure 3**). The sandwich interfaces helped a lot accelerate charge transport and separation and benefit the activation of CO_2 photoreduction.[33] In another study, negatively charged $ZnIn_2S_4$ and positively charged $MoSe_2$ attracted each other via robust electrostatic attraction. The atomic interface formed in this way endowed a remarkably improved photocatalytic hydrogen generation performance.[34] The electrostatic interaction was ascribed to the first-step formation of the graphene/CdS interface in Jung's work, and then, the

Table 1. Examples of devised approaches to fabricating atomic interfaces in chalcogenides.

Atomic interfaces in chalcogenides	Formation approaches	Reference
CdS/Ti_2C_3	self-assembly	[31]
CeO_x-S/$ZnIn_2S_4$	self-assembly	[32]
$ZnIn_2S_4$/In_2O_3	self-assembly	[33]
$ZnIn_2S_4$/$MoSe_2$	self-assembly	[34]
CdS/rGO	self-assembly	[35]
MoS_2/SnS_2/rGO	self-assembly	[36]
CdS/MoS_2	S-vacancies-induced S-metal bonds	[40]
$ZnIn_2S_4$/$MoSe_2$	S-vacancies-induced S-metal bonds	[41]
$ZnIn_2S_4$/MoS_2	S-vacancies-induced S-metal bonds	[42]
$CuGaS_2$/ZnS	Cation exchange	[43]
$Co_{0.85}Se$-CdSe/$MoSe_2$/CdSe	Cation exchange	[44]
In_2S_3/$CuInS_2$	Cation exchange	[45]
CdS/PbS	Cation exchange	[46]
CdSe/CdS	Epitaxy	[49]
ZnSe/ZnS	Epitaxy	[50]
CdSe/PbS	Epitaxy	[51]
SnS_2/SnO_2	Epitaxy	[52]
SnS_2/WS_2	Epitaxy	[53]
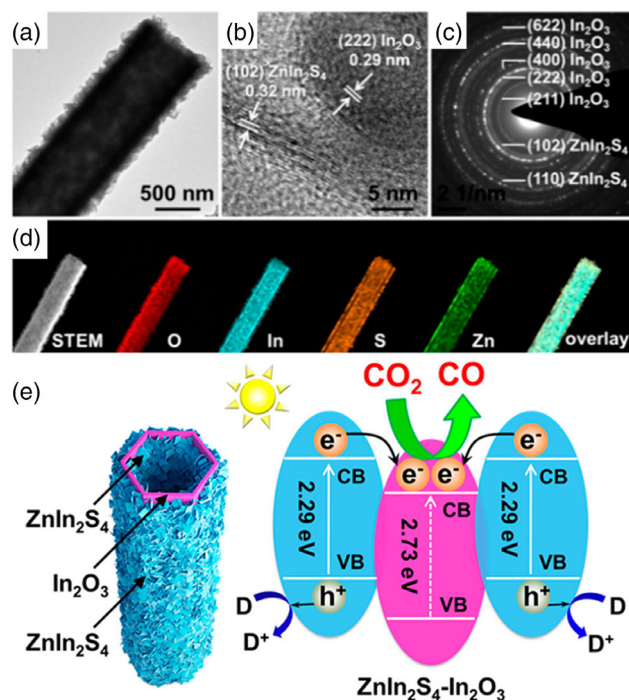
Figure 3. a) The transmission electron microscope (TEM) image, b) the high-resolution TEM (HRTEM) image, c) the selected area electron diffraction (SAED) patterns, and d) energy dispersive spectrometer (EDS) mapping of $ZnIn_2S_4$/In_2O_3 hierarchical microtubes. e) The illustration of the $ZnIn_2S_4$/In_2O_3 interface and the charge transport across the sandwich-like interfaces for boosting photoreduction of CO_2. Reproduced with permission.[33] Copyright 2018, American Chemical Society.

amine-functionalization of graphene donated to further uniformly wrapped and large-area interfaces.[35] Comparison experiments told the enhancement in charge separation across the atomic interface after being amine-functionalized, which exhibited a 3.5-time and 20-time amendment in CO_2 to methane rate under 1 and 0.1 bar, respectively. Another effort designed a ternary $MoS_2/SnS_2/rGO$ hybrid for photoinduction of CO_2, where MoS_2 assembled onto rGO (reduced graphene oxide) and SnS_2 thanks to the weak van der Waals interactions.[36] The large surface area and surface functional groups were proved to strengthen the joint influence of the atomic interface.

3.2. Anion Vacancy-Induced VI–Metal Bond

As chalcogens with p-orbitals have a larger orbital extension and a closer match in terms of energy to transition metals with d-orbitals, there is more space to tailor their electronic properties via orbital hybridization.[37] Anion vacancies, which are initiated from the escape of VI atoms from chalcogenides lattices, especially sulfur vacancies are more easily engendered owing to lower formation energy and lower stability.[38] Sulfur atoms in chalcogenides show higher electronegativity compared with the other metal atoms in the lattice. A theoretical simulation has also predicted that the surface sulfur vacancies will manufacture spontaneously.[39] High-temperature treatment, high-energy plasma, ion/electron irradiation,[22c] vacuum treatment, and chemical reduction via reducing reagents are several effectual protocols for controlling the removal of S, Se, or Te lattice atoms. Once the VI vacancies are created, the charge density of the surrounding coordinated atoms will be changed, and other VI atoms will also be different in coordination numbers and electronic structures. These changes triggered by anion vacancy defects provide channels for potent bonds with other semiconductors and controllable interface growth.

Early in 2017, it has been unveiled that MoS_2 ribbon could directionally and coaxially grow on CdS nanowires owing to surface and subsurface defects caused by hydrazine hydrate in a high-temperature treatment. The interatomically Cd–S (S in MoS_2) bond was a result of Cd^0 nucleation sites and S vacancies in CdS (**Figure 4**a,b).[40] The wonderful lattice match of about 99.7% between planes of CdS and MoS_2 was also investigated in this work (Figure 4c). The delocalized interface states between CdS and MoS_2 expedited charge transport across this atomic interface and thus provided a dramatically enhanced H_2 generation performance with an apparent quantum yield (AQY) of 79.7% at 420 nm. The developed fashion offered new insights as to how chalcogenides electrocatalysts can be combined with other chalcogenides semiconductors. Li and colleagues ingeniously constructed a kind of interface with intense interfacial chemical bonds in a $ZnIn_2S_4/MoSe_2$ hybrid. By virtue of the strong reductive ability of hydrazine monohydrate, abundant S vacancies were formed in $ZnIn_2S_4$ during a hydrothermal procedure. After that, an atomic interface between $ZnIn_2S_4$ and $MoSe_2$ was then in situ fabricated since the coordinative unsaturation of S atoms caused by S vacancies contributed a significant role in the anchoring of Mo atoms from $MoSe_2$. The Mo–S bond was the pivotal precondition for this atomic interface.[41] Both the decreased electron paramagnetic resonance (EPR) signals of S

vacancy and the shift of X-ray photoelectron spectroscopy (XPS) peaks, as well as the new Raman peak observed in $ZnIn_2S_4/MoSe_2$ hybrid, verified that it was the Mo–S bond that provoked the atomic-scale intense interface (Figure 4d). This effort gave an inspiring example for the design of atomic interface in chalcogenides and the further modulation of charge transfer. In another study, MoS_2 quantum dots (QDs) incorporated with monolayered $ZnIn_2S_4$ stimulated by S vacancies on a Zn facet, and the preparation process is depicted in Figure 4e shown.[42] S vacancies caused a more intensive positive charge density around the circumambient Zn atoms, which was suggested by the electronic structure calculations. Consequently, a significant link between the electronic manipulation and photocatalysis activities of this hybrid was established. This atomic level $ZnIn_2S_4/MoS_2$ interface sparked a steered charge flow with a low edge contact barrier and a significant expansion in photocatalytic H_2 generation (Figure 4f). An average H_2 evolution rate of 6.884 mmol g^{-1} h^{-1} and an AQY of 63.87% at 420 nm were detected from this hybrid with an atomic interface.

3.3. In Situ Cation-Exchange-Induced Atomic Interfaces

Some embedded cations show a relatively weak bond with anion lattices or locate at accessible sites, subsequently being more exchangeable with other free cations. Furthermore, the inorganic anion VI frameworks maintain stability during a proper cation exchange. The in situ cation exchange would contribute to the formation of the solid solution of chalcogenides as well as a new solid phase extended on the basis of the original phase. Thus, the atomic interfaces with shared anionic lattice will be formed.

The $CuGaS_2$–ZnS interface was designed by a multistep cation exchange strategy in a previous investigation.[43] The authors ingeniously employed $Cu_{1.94}S$ nanocrystals as the initial assistants for the surface growth of ZnS, and then they sacrificed them to further introduce $CuGaS_2$ into the heterojunction. As shown in **Figure 5**a–g, the formation process of zigzag $CuGaS_2/ZnS$ was monitored via the transmission electron microscopy (TEM) observation. With increased reaction time, wedge-shaped $CuGaS_2$ appeared and was situated at the interface between $Cu_{1.94}S$ and ZnS until $Cu_{1.94}S$ vanished. The constant angle of ≈44° originated from the couple of crystal planes, where afresh generated $CuGaS_2$ phase provided its $(10\bar{1}0)$ plane to couple with $Cu_{1.94}S$ while its (0002) plane coupled with ZnS. Tian and coworkers rationally designed a kind of $Co_{0.85}Se$–CdSe/$MoSe_2/CdSe$ sandwich-like cages involving multi-junctions and diverse interfaces.[44] After the formation of $Co_{0.85}Se$ polyhedron cages via a selenylation procedure, $MoSe_2$ was loaded outside the hollow $Co_{0.85}Se$ cages during the high-temperature solvothermal progress. Afterward, the cation exchange successfully occurred between the Mo^{4+} in the $MoSe_2$ substrate lattice and the Cd^{2+} dissolved in the ascorbic acid solution (Figure 5h). Noteworthy, ascorbic acid played a key role in the exchange from $Co_{0.85}Se$ to CdSe; meanwhile, $MoSe_2$ also served as a critical bridge to connect the two kinds of selenium on both sides. The atomic interfaces between these three chalcogenides were reported to be gratifying for the remarkably improved
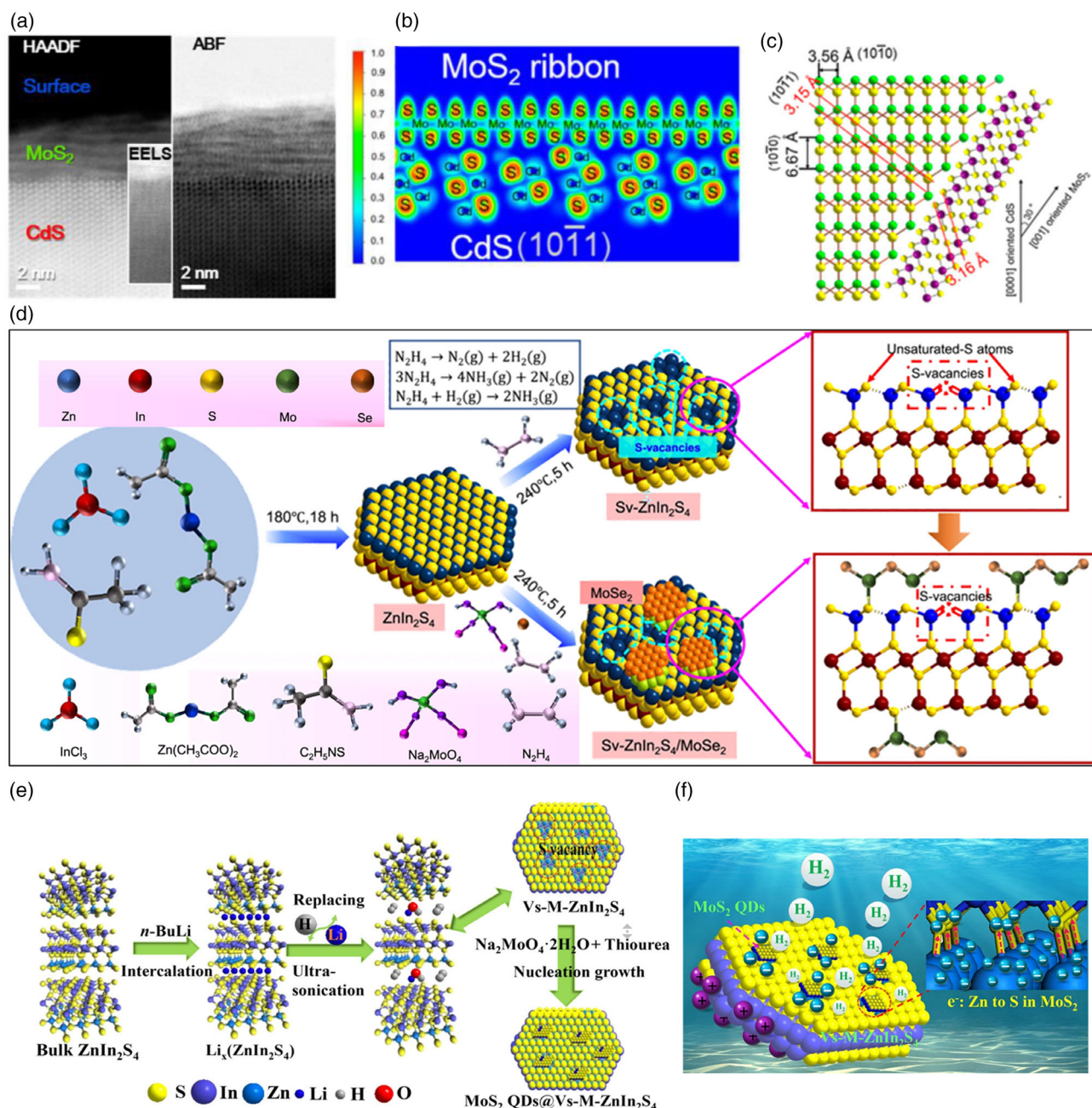
Figure 4. a) High-angle annular dark–field (HAADF) and annular bright-field (ABF) scanning transmission electron microscopy (STEM) images at the CdS/MoS₂ interface. b) The calculated electron localization function (ELF) of the interfacial CdS and MoS₂. c) The proposed schematic model of the growth of MoS₂ at the CdS interface. Reproduced with permission.[40] Copyright 2017, American Chemical Society. d) The schematic illustration of the formation of $ZnIn_2S_4$ with abundant S vacancies and the atomic interface of $ZnIn_2S_4$ and $MoSe_2$. Reproduced with permission.[41] Copyright 2021, Springer Nature. e) The illustration of the preparation of $ZnIn_2S_4$ and the directed growth of MoS_2 by S vacancies. f) The schematic mechanism for photocatalytic H_2 generation in $ZnIn_2S_4/MoS_2$ hybrid with atomic interfaces devoted by S vacancies. Reproduced with permission.[42] Copyright 2018, American Chemical Society.

performance for photocatalytic CO_2 reduction. In another study, an atomic interface between In_2S_3 and $CuInS_2$ was designed by a beforehand sulfidation and ion exchange.[45] The results demonstrated that the Cu^{2+} cation in the precursor solution could replace the In^{3+} at the surface of In_2S_3, thus an atomic interface was subsequently formed with intense bonds. A kind of Cd/Pb

chalcogenide Janus hybrid was developed through the controllable cation exchange in early work.[46] The process of exchanging the Cd^{2+} cation for the Pb^{2+} cation could be controlled by altering both the reaction temperature and period. In addition, the thermally activated characteristic and the anisotropy for exchange were highlighted, where the cation exchange started from the
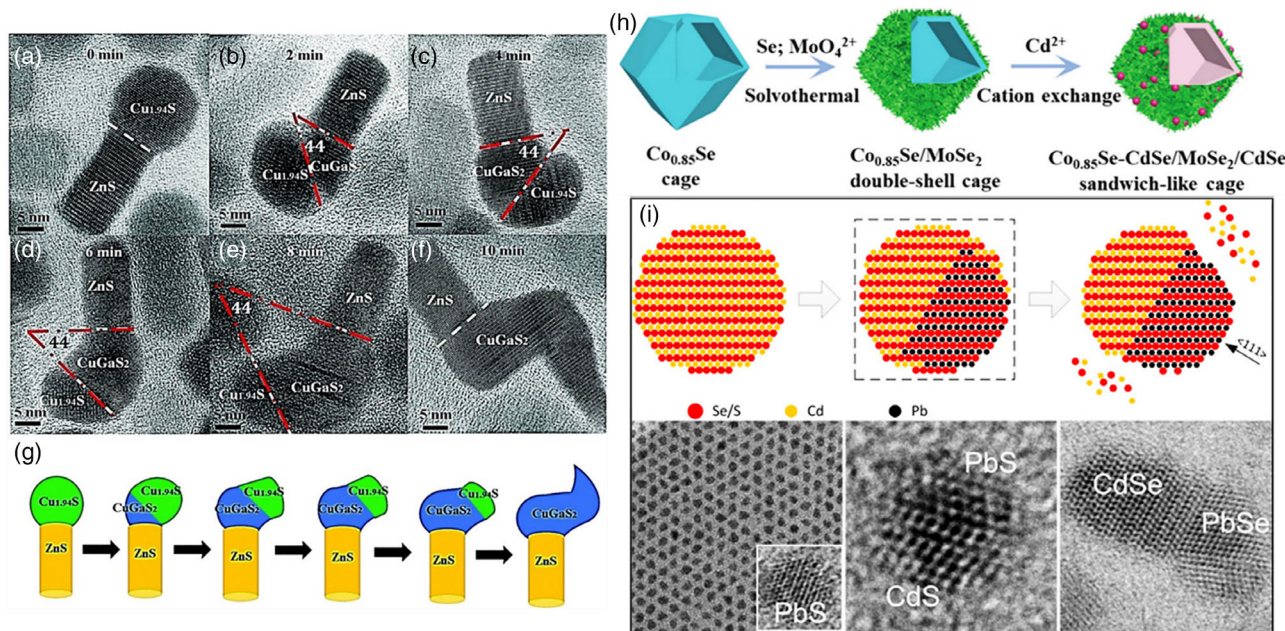
Figure 5. a–f) The high-resolution TEM (HRTEM) images of CuGaS$_2$/ZnS (Cu$_{1.94}$S) hybrids were observed with increased reaction time for cation exchange. g) Schematic illustration of the formation from Cu$_{1.94}$S/ZnS to CuGaS$_2$/ZnS via the cation exchange strategy. Reproduced with permission.[43] Copyright 2016, The Royal Society of Chemistry. h) The synthesis of hierarchical Co$_{0.85}$Se–CdSe/MoSe$_2$/CdSe polyhedron cages via in situ cation exchange. Reproduced with permission.[44] Copyright 2021, Wiley-VCH. i) The proposed direction-dependent model for Cd^{2+} cation exchanged to Pd^{2+} and the TEM images of Cd/Pb chalcogenides. Reproduced with permission.[46] Copyright 2015, American Chemical Society.

edge and proceeded along the <111> direction generating a sharp atomic interface at the (111) crystallographic plane (shown in Figure 5i).

3.4. Slow Epitaxy Atomic Interfaces

Some chalcogenides possess similar symmetry and lattice constants, which provide favorable conditions for epitaxial growth or epitaxial assembly. Rational crystal facet design and crystal-orientation guidance will result in smaller lattice mismatches and higher interfacial stability. In addition, 2D nanomaterials also show an epitaxial relationship due to the van der Waals force, which is termed van der Waals epitaxy.[47] A pioneering investigation indicated the van der Waals epitaxy between MoS$_2$ and graphene.[48] Apart from van der Waals epitaxy, the epitaxy growth of chalcogenides relies on shared elements, orientation match, and slow rates.

An epitaxial interface was formed based on CdSe nanoplatelets via the epitaxial growth of CdS wings with an atomic observation of a Se-containing core surrounded by an S-containing region.[49] In a previous report, ZnSe/ZnS core–shell interface was prepared in the quantum rod morphology.[50] Similarly, the epitaxial interface of the CdSe/PbS core/shell structure was designed with a crystal structure mismatch. It was implied that the absorption properties were closely related to the interface growth.[51] The SnS$_2$ layer was anchored on the SnO$_2$ hollow spheres through an epitaxial way being soaked in a high-temperature hydrothermal environment.[52] The epitaxy growth of SnS$_2$ originated from partial sulphuration of SnO$_2$, thus the ratio of hybridization and the shell numbers could be easily

adjusted by the reaction period. As shown in **Figure 6**, Wang et al. synthesized single-, double-, triple-, and quadruple-shelled hollow SnS$_2$/SnO$_2$ junctions with epitaxial interfaces. They proposed an epitaxy model for this kind of atomic interface after investigating the phase structures of SnS$_2$ and SnO$_2$. From this atomic-scale model, it could be extracted that there was a lattice distortion located at the interfaces, which was unveiled to enhance light utilization and charge separation for boosting photoreduction CO$_2$ 100% selectively to CO. Differently, WS$_2$ was epitaxially deposited on SnS$_2$ and their interface was occupied by a new metallic Sn$_{0.5}$W$_{0.5}$S$_2$ phase, which afforded rapid charge transport across interface.[53]

4. The Role of Atomic Interfaces in Chalcogenides for Photocatalysis

As mentioned in Introduction provided earlier, chalcogenides contain a vast and diverse set of semiconductor materials owing to their large extended states of energy bands, which correlate with binary, ternary, quaternary, and more multinary metal chalcogenides. There have been studies reviewing the properties of ternary and quaternary metal chalcogenides.[54] All these diversities stem from the gradually increased elements permeating into the chalcogenides photocatalysts family, and the main involved VI elements and metal elements are listed in **Figure 7**. Turning now to the roles of designing atomic interfaces in chalcogenides-based photocatalytic systems, the rich elemental composition predestined the various initial energy band structures. In a typical hybrid architecture, light absorbers, electron–holes-generating hosts, carriers transport mediums, and catalytic reaction
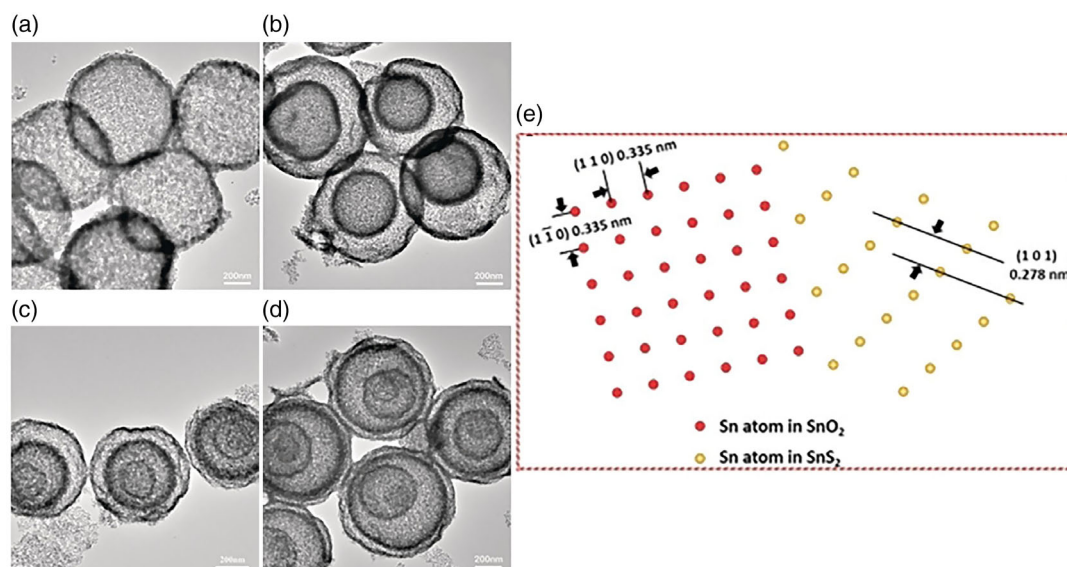
Figure 6. TEM images of a) hollow spheres, b) double, c) triple, and d) quadruple-shelled SnS_2/SnO_2 hollow spheres; e) the proposed atom arrangement model at the epitaxial interface between SnS_2 and SnO_2. Reproduced with permission.[52] Copyright 2020, Wiley-VCH.
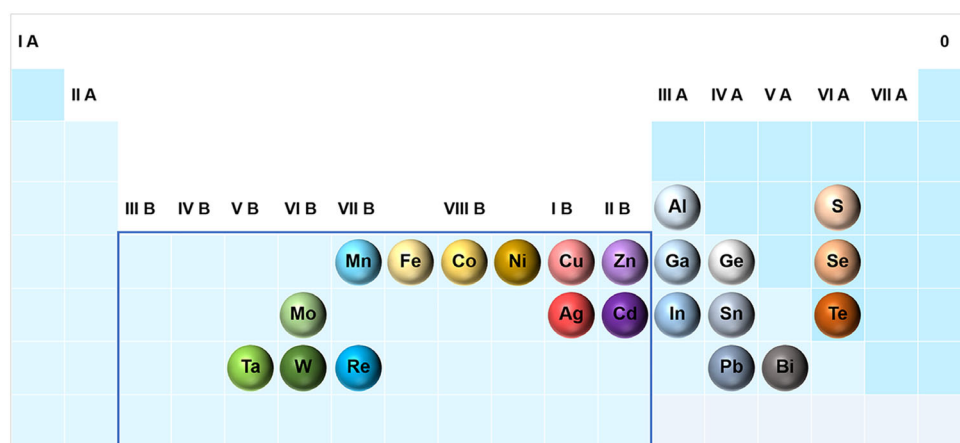

Figure 7. A list of main involved elements which consist of chalcogenides-based photocatalysts.

activators orchestrate with each other to exhibit an integrated photocatalytic performance. These functions strongly depend on the energy band structures of branches in the hybrids. Undoubtedly, the functions of each part cannot be simply distinguished as a component may perform diverse distinct functions. In simple terms, the predominant photocatalyst is responsible for light absorption along with the generation of photoinduced electron–hole pairs, while a co-catalyst is for the activation of photocatalytic reactions. Notably, interfaces in chalcogenides also devote to the functions apart from the linked phases. To make a real difference in photocatalysis, interfaces must be established properly and moderately, since excessive interfaces will form reassembly centers and cause carriers to recombine.[55] In addition, light absorption and surface activation may be inhibited by excessively distributed interfaces. Herein, from the contributions of chalcogenides in photocatalytic devices, the contribution of atomic interfaces can be distinguished and described by inventorying recent related advances. Here, we place our focus

exclusively on the photocatalytic process, where the surface redox reactions are only driven by solar energy without applying any bias in a heterogeneous suspended particle system. **Figure 8** provides an overview of the roles of atomic interfaces in chalcogenides-based photocatalysts based on the three functions of chalcogenides: predominant photocatalysts, the supports of single atoms, and co-catalysts.

4.1. Chalcogenides as Predominant Photocatalysts

Early interests in photocatalysis applications are located at CdS, ZnS, and other binary metal chalcogenides. However, the monotonicity of elements restricts the further rendering of optical and electrical properties. The tunability of multimetallic chalcogenides makes them appealing as the activated absorber moiety on the photocatalyst hybrid. Quaternary sulfide crystallines, such as Zn-based and Cu-based multinary sulfides, present increasingly available visible-light-driven predominant photocatalysts
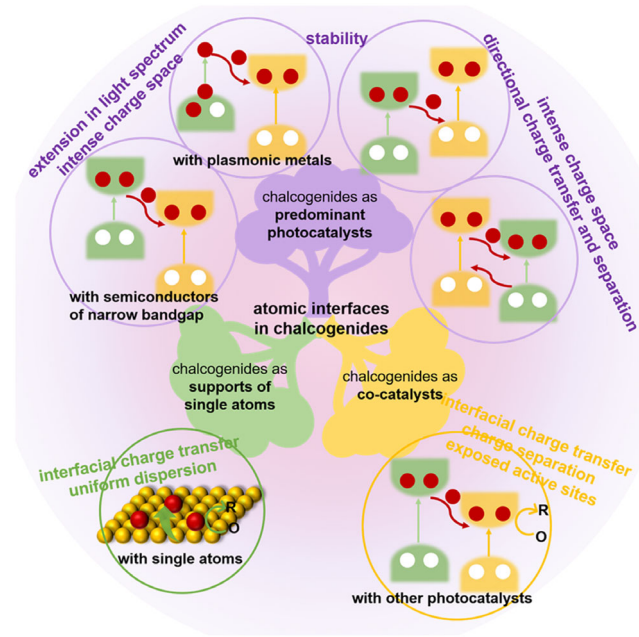
Figure 8. The roles of atomic interfaces in photocatalysis when chalcogenides serve as the predominant photocatalysts, the supports of single atoms, and co-catalysts, respectively.

with environmental-benign characteristics. More eye-etching, several kinds of plasmonic metal chalcogenides (Cu–VI, Hg–VI, VI=S, Se, or Te) have been widely investigated for their fascinating vacancy-dependent LSPR effect and accessible spectral response range from visible to near-infrared (NIR) range.[56] The particular attraction of plasmonic nonstoichiometric/degenerately doped copper chalcogenides for the broadened spectral domains and regulated optoelectronic properties sparks increasing well-articulated reviews, which meticulously expound the association of composition, morphology, plasmonic properties, and potential applications.[56a,57] Merits of tunable surface localized electromagnetic field and extended light-harvesting render plasmonic metal chalcogenides a class of promising photocatalysts.[58] For alleviating the disadvantage of limited photocatalytic performance due to the narrow bandgap of plasmonic chalcogenides,[59] hybridization with other semiconductor photocatalysts or metals behaves as a powerful platform.[25,60] Atomic interfaces built in this way as well as their roles are also selectively covered in this section. **Table 2** summarizes the intense bonds as bridges of atomic interfaces in chalcogenides with ameliorated performance with respect to diverse photocatalysis applications.

4.1.1. Intense Charge Space and Directional Charge Transport

At the interface, charges are prone to redistribute owing to the obvious electronic interaction between the different energy band structures of adjacent phases.[61] For this reason, the internal electric field with intense charge space is kinetically built with an extraordinary capacity to maneuver expected charge separation.[62] We here discuss the intense charge space from the feasible Z-scheme and type II interface shown in Section 2. The Z-scheme (or similar S-scheme) junctions and type II

junctions are well acknowledged for their ordered intense charge spaces at the interfaces in the field of photocatalysis. At this time, charge carriers migrate according to a predetermined path as long as there is intimate interfacial contact across the interface.

Z-scheme interfaces are designed to maintain the merit that photoinduced electrons and holes present stronger reduction and oxidation capability, respectively, and thus the active redox sites are spatially located on different semiconductors.[63] In Li's report, the atomic interface connected by the robust Mo–S bonds between $ZnIn_2S_4$ and $MoSe_2$ was highlighted along with the generated interfacial internal electric field.[41] The authors claimed the hindrance of poor interfacial connection to charge transport. They regarded the interfacial atomic chemical bonds as a special "bridge" to accelerate charge flow across adjacent components. The benefit of this atomic interface has also been disclosed by the comparison of hydrogen evolution performance with the physical mixture of $ZnIn_2S_4$ and $MoSe_2$. The optimal $ZnIn_2S_4/MoSe_2$ hybrid with atomic interface bonded by Mo–S bond showed a prominent HER rate of 63.21 mmol $g^{-1} h^{-1}$, while the physical mixture of $ZnIn_2S_4$ and $MoSe_2$ by ultrasound possessed inferior performance, as shown in **Figure 9**a. The atomic interface obstructed the charge reassembly process via a Z-scheme mechanism (Figure 9b). The tightness and stability of the atomic interfaces for the successful operation of the S-scheme hybrid were underlined using a CdS/SnO_2 configuration.[64] An interfacial lattice match was observed between CdS and SnO_2, which was identified to be the pivotal insurance to the fabrication of the atomic interface. Charge redistribution and the stimulated intense charge space at the CdS/SnO_2 atomic interface accounted for the directional carrier migration following an S-scheme way (Figure 9c). Therefore, an optimal H_2 generation performance 5 times higher than pure CdS was obtained eventually. Another kind of direct Z-scheme interface was fabricated between $ZnIn_2S_4$ and CdS (Figure 9d) and showed a superior visible-light-driven H_2 evolution performance as well as excellent photochemical stability during the continuous photocatalytic test of 20 h.[27] The authors confirmed the Z-scheme interface from both the experimental and density-function theory (DFT) calculation aspects. The calculated 3D charge density difference at the $ZnIn_2S_4/CdS$ interface unveiled enriched electron clouds and a stronger competence to enrich electrons at the $ZnIn_2S_4$ side, demonstrating the directional electron-transfer trend from CdS to $ZnIn_2S_4$ and illustrating the interfacial Z-scheme mechanism. In addition, from the electrostatic potential of the $ZnIn_2S_4/CdS$ interface, an electrophilic character was found in CdS while $ZnIn_2S_4$ exhibited to be the nucleophilic one, revealing the same tendency for the accumulation of electrons and holes at $ZnIn_2S_4$ side and CdS side, respectively. Detailed observations identified the vital role of this atomic interface for all the involved advantages to boost photocatalytic H_2 generation, including facilitated charge separation and transport, improved light absorption, abundant active sites, and sound reaction stability. A Z-scheme atomic interface was also developed between $ZnIn_2S_4$ with WO_3 for water splitting. The interfacial tungsten–sulfur (W–S) bonds and the intense electric field jointly facilitated charge separation and a high H_2 evolution rate of 11.09 mmol $g^{-1} h^{-1}$.[65] The Z-scheme mechanistic pathway was also observed in the $In_{2.77}S_4/$ porous organic polymer (POP) hybrid for transforming CO_2 to ethylene driven by light

Table 2. The collected atomic interfaces in chalcogenides and their roles for diverse boosting photocatalysis applications.

| Interfaces of chalcogenides	Applications	Performances	Roles of atomic interfaces	Reference
CeO_x-S/$ZnIn_2S_4$	CO_2 reduction	CO productivity of 0.18 mmol g^{-1} h^{-1}	Trapping electrons, activating reactant	[32]
$ZnIn_2S_4$/In_2O_3	CO_2 reduction	CO yield of 3075 µmol g^{-1} h^{-1}	Accelerating charge separation and transport, offering a large surface area for CO_2 adsorption, exposing abundant active sites	[33]
MoS_2/SnS_2/rGO	CO_2 reduction	CO and CH_4 formation rate of 68.53 and 50.55 µmol g^{-1} h^{-1}	Facilitating multilevel charge transport, prolonging carriers' lifetime, exposing more active sites	[36]
$Co_{0.85}Se$-CdSe/$MoSe_2$/CdSe	CO_2 reduction	CO yield of 15.04 µmol g^{-1} h^{-1}, 90.14% selectivity	Accelerating charge transport and separation, improving visible light utilization, increasing catalytic active sites	[44]
In_2S_3/$CuInS_2$	CO_2 reduction	CO evolution rate of 19.00 µmol g^{-1} h^{-1}	Inhibiting charge recombination, enhancing reactant absorption, providing active sites	[45]
SnS_2/SnO_2	CO_2 reduction	CO evolving rate of 48.01 µmol g^{-1} h^{-1}, a 100% selectivity of CO_2-to-CO	Providing active sites, improving charge separation	[52]
$In_{2.77}S_4$/POP	CO_2 reduction	C_2H_4 generation rate of 67.65 µmol g^{-1} h^{-1}, 98% selectivity	Z-scheme electron transfer, improving charge separation	[66]
Au@Pt/CdS/C_3N_4	CO_2 reduction and H_2 evolution	A H_2 evolution and CO_2 reduction of ≈17.2 and ≈14.3 times higher than that of CdS/C_3N_4	Improving light harvesting and charge utilization, accelerating charge transfer and separation	[70]
$CuGaS_2$/CdS	CO_2 reduction	A fourfold higher rate of CO_2-to-CO than $CuGaS_2$ and threefold than CdS	Improving stability and charge separation	[79]
CdS/TiO_2: Cu	CO_2 reduction and H_2 evolution	CO yield of 781.3 µmol g^{-1} h^{-1} and a H_2 evolution rate of 5875.1 µmol g^{-1} h^{-1}	Increasing stability and charge separation	[80]
CdSe/CdS	CO_2 reduction, oxidative organic synthesis	CO transition rate of ≈412.8 mmol g^{-1} h^{-1}, a selectivity of >96%	Improving light response and charge separation, enhancing the selectivity of pinacol production	[83]
$CuIn_5S_8$/$MoSe_2$	CO_2 reduction	CO and CH_4 output of 30.4 and 14.7 µmol g^{-1}	Improving charge separation	[111]
CdSe/ZnSe	CO_2 reduction	CO yield of 25.6 mmol g^{-1} h^{-1}	Increasing light absorption, promoting charge separation	[112]
SnS_2/g-C_3N_4	CO_2 reduction	CH_3OH yield of 2.3 µmol g^{-1}, CH_4 yield of 0.64 µmol g^{-1}	Realizing a Z-scheme electrons pathway	[113]
CuInZnS/g-C_3N_4	CO_2 reduction	CO yield of 50.04 µmol g^{-1}	Enhancing light absorption and charge separation	[114]
Co_9S_8@$ZnIn_2S_4$/CdS	CO_2 reduction and H_2 evolution	CO yield of 82.1 µmol g^{-1} h^{-1}, H_2 evolution of 1419.14 µmol g^{-1} h^{-1}	Improving carrier separation and utilization, broadening light absorption	[115]
Co/MoS_2	Hydrodeoxygenation of 4-methylphenol to toluene	Reducing reaction temperature from 300 to 180 °C	Realizing superior activity, selectivity, and stability	[87]
Mo/MoS_2	Hydrodesulfurization	2–3 times of HDS activity than CoMoS catalysts	Improving catalysis activity	[88]
Cu_7S_4/Pd	Organic synthesis reactions	80%–100% conversion within 2 h	Facilitating charge transfer, retaining NIR light utilization	[60]
$ZnIn_2S_4$/$MoSe_2$	H_2 evolution	H_2 yield of 6454 µmol g^{-1} h^{-1}	Accelerating charge separation and transport, increasing stability	[34]
CdS/MoS_2	H_2 evolution	An AQY of 79.7% at 420 nm, 53.1% at 450 nm, and 9.67% at 520 nm	Facilitating charge transport, passivation of surface trap state	[40]
$ZnIn_2S_4$/$MoSe_2$	H_2 evolution	A yield of 63.21 mmol g^{-1} h^{-1}, AQY of 76.48% at 420 nm	Accelerating charge separation and transport via a Z-scheme route	[41]
$ZnIn_2S_4$/MoS_2	H_2 evolution	A yield of 6.884 mmol g^{-1} h^{-1}, AQY of 63.87% at 420 nm	Steering charge flow, decreasing contact resistance	[42]

Table 2. Continued.

Interfaces of chalcogenides	Applications	Performances	Roles of atomic interfaces	Reference
$CuGaS_2/ZnS$	H_2 evolution	A yield of 131 μmol g^{-1} h^{-1}, 15 times higher than $CuGaS_2$	Accelerating charge separation and transport	[43]
CdS/SnO_2	H_2 evolution	A yield of 2.54 mmol g^{-1} h^{-1}, 5 times higher than CdS	Enhancing charge separation and optimal surface reaction	[64]
$ZnIn_2S_4/CdS$	H_2 evolution	H_2 yield of 7.4 mmol g^{-1} h^{-1}, AQY of 12.6% at 420 nm	Improving light harvesting, facilitating charge separation, shortening charge-transfer distance to the surface	[27]
$ZnIn_2S_4/WO_3$	H_2 evolution	A yield of 11.09 mmol g^{-1} h^{-1}, an AQY of $\approx$72% at 420 nm	Facilitating charge separation via the Z-scheme mechanism	[65]
$ZnS/CdIn_2S_4/rGO$	H_2 evolution	H_2 generation rate of 6.82 mmol g^{-1} h^{-1}, an AQY of 19.34%	Enhancing spatial charge separation and light harvesting, exposing more active sites	[67]
$MoS_2/Cu-ZnIn_2S_4$	H_2 evolution	H_2 yield of 5463 μmol g^{-1} h^{-1}, an AQY of 13.6%	Improving charge transport and separation	[68]
$ZnMoS_4/ZnO/CuS$	H_2 evolution	H_2 yield of 38.22 mmol g^{-1} h^{-1}, 97% improvement than $ZnMoS_4/CuS$	Directing desired charge migration	[69]
$CdS/CoP@AAH$	H_2 evolution	H_2 yield of 54.9 mmol g^{-1} h^{-1}, an AQY of 40.62%	Improving stability and charge separation	[81]
$Au@MoS_2/CdS$	H_2 evolution	H_2 yield of 29.6 mmol g^{-1} h^{-1}, an AQY of 35.7% at 450 nm, and an AQY of 1.06% at 700 nm	Extending light spectrum to the NIR region, improving charge separation, behaving as active sites	[82]
$ZnIn_2S_4/MoSe_2$	H_2 evolution	H_2 yield of 2228 μmol g^{-1} h^{-1}, an AQY of 21.39% at 420 nm	Electrons storage and active sites	[94]
$CdS/MoO_2/MoS_2$	H_2 evolution, pyruvic acid synthesis	An AQY of 11.3% at 420 nm, 29% conversion of lactic acid, 95% selectivity of PA	Facilitating charge separation, prolonging carriers' lifetime	[95]
CoS/CdS	H_2 evolution	A rate of 65.7 mmol g^{-1} h^{-1}	Interfacial charge rearrangements, reducing thermodynamic energy barriers, improving carrier separation	[96]
$NiPS_3/CdS$	H_2 evolution	A yield of 13.6 mmol g^{-1} h^{-1}	Facilitating charge transport and dissociation, exposing active sites	[97]
CuS/CdS	H_2 evolution	A yield of 561.7 μmol g^{-1} h^{-1}	Promoting charge dissociation, providing active sites	[100]
$Mn_{0.2}Cd_{0.8}S/MoS_2$	H_2 evolution and CO_2 reduction	H_2 rate of 335.02 μmol h^{-1} and a CH_3OH rate of 2.13 μmol h^{-1}	Facilitating charge transfer and separation, improving stability	[116]
CdS-fullerene/graphene	H_2 evolution	The yield of 127.2 μmol h^{-1} g^{-1}, AQY of 7.24% at 420 nm	Ultrafast interfacial charge transfer, prolonging carriers' lifetime	[109]
Cu–In–Zn–S/MoS_2/CDs	H_2 evolution	A yield of 3706 μmol h^{-1} g^{-1}, 6.65 times to pure Cu–In–Zn–S	Facilitating charge transport, exposing active sites	[108]
$PtP_2@C/CdS$	H_2 evolution	A yield of 9.76 mmol h^{-1} g^{-1}, an AQY of 41.67% at 420 nm	Enriching active sites	[117]
CuS/Au	Degradation of RhB	98.81% RhB degraded within 1 h, 2.27 times higher than CuS	Achieving coupling effect of near-filed enhancement and resonance energy transfer	[30]
CuS/ZnO	Degradation of MB	Almost 100% MB degraded within 20 min with a rate constant of 0.18 min^{-1}	Improving light utilization, charge transfer, and recyclability	[59a]
$MoSe_2$/CDs	Degradation of Cr(VI)	More than 99% degradation	Accelerating charge separation, extending light absorption	[74]
CuS/g-C_3N_4	Degradation of Rhodamine B	Degradation rate of 0.02892 min^{-1}, 15-time improvement than g-C_3N_4	Accelerating charge separation and transport	[84]
CuS/ZnO	Degradation of TC	85.28% TC degraded	Achieving photo-piezoelectric synergistic catalysis effect, providing a driving force for charge migration	[85]

Table 2. Continued.

Interfaces of chalcogenides	Applications	Performances	Roles of atomic interfaces	Reference
$CuS/BaTiO_3/Ti_{32}$-oxo-cluster	Degradation of TC	≈100% TC degraded within 60 min	Achieving photo-piezoelectric synergistic catalysis effect, accelerating charge transfer, utilizing visible light	[86a]
$CuS/BaSO_4$	Degradation of TC	Degrading kinetic constant of 0.014 min^{-1}	Serving as a special channel for charge transfer, activating insulator	[86b]
$CuSe/CaCO_3$	Decomposition of 4-nitrophenol (4-NP) and bacteria	Degrading 4-NP kinetic constant of 0.4843 min^{-1}	Serving as a special channel for charge transfer, activating insulator, broadening spectrum response	[86c]
Pd/CdS	N-alkylation of amines with alcohol	100% aniline conversion, an almost 100% selectivity, H_2 yield of 11.8 $mmol\,g^{-1}\,h^{-1}$	Prolonging carriers' lifetime, trapping photoinduced electrons	[92]
$BaTiO_3@ReS_2$	Degradation of RhB	An apparent degradation rate of 0.133 min^{-1}	Reducing transfer resistance, enhancing oxygen activation capacity	[99]
In_2S_3/TiO_2	H_2O_2 production	H_2O_2 yield of 376 $\mu mol\,L^{-1}\,h^{-1}$	Promoting charge separation	[118]
$ZnO/ZnSe/MoSe_2$	Degradation of MO, sterilization of *Escherichia coli*	91.5% MO degradation, 4.97 log *Escherichia coli* inactivation in 120 min	Ensuring a gradual charge transfer, improving visible light utilization	[119]
$MoSe_2/Bi_2WO_6$	Oxidation of gaseous toluene	Near 80% degradation, 7 times higher than $MoSe_2$	p–n heterointerface, prolonging carriers' lifetime	[120]
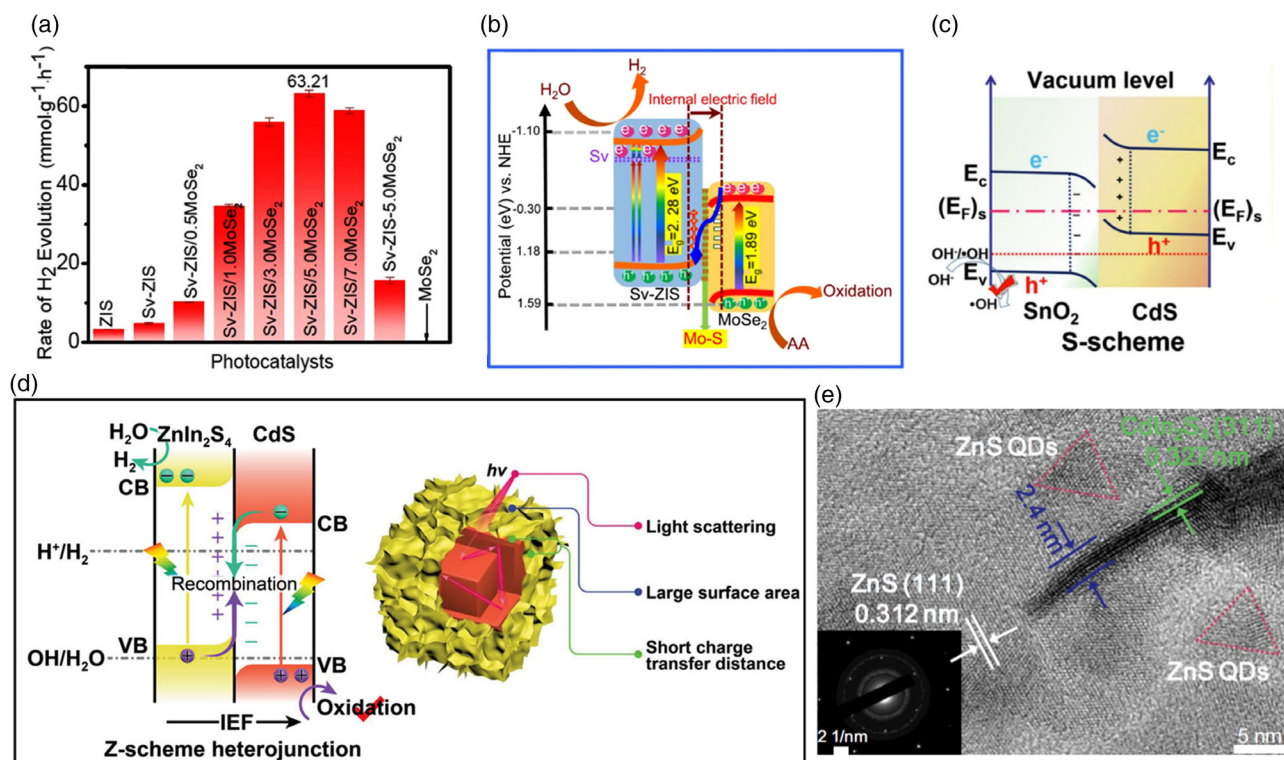
Figure 9. a) Hydrogen evolution reaction (HER) performance of $ZnIn_2S_4/MoSe_2$ with interfacial Mo–S bonds, the mixture of $ZnIn_2S_4$–$MoSe_2$, and single branches. b) The intense charge space and internal electric field that was distributed across the atomic interface of $ZnIn_2S_4/MoSe_2$. Reproduced with permission.[41] Copyright 2021, Nature Publishing Group. c) The S-scheme charge-transport mechanism of the CdS/SnO_2 interface and the proposed photocatalytic progress. Reproduced with permission.[64] Copyright 2022, Elsevier. d) The Z-scheme interfacial charge transport and the integral effect of $ZnIn_2S_4$/CdS photocatalyst. Reproduced with permission.[27] Copyright 2022, Wiley-VCH. e) The HRTEM images of ZnS/$CdIn_2S_4$/rGO nanocomposite. Reproduced with permission.[67] Copyright 2017, Elsevier.

illumination.[66] Aside from the four-coordinated In^{2+} and six-coordinated In^{3+} surface active centers, the synergistic influence of the Z-scheme interface, which was developed via polarity-driven electrostatic attraction, contributed to the overall photocatalytic performance transferring CO_2 to C2 product. In this study, the Z-scheme atomic interface was precisely proved by a series of approaches, including analysis of band structure and surface reactions, the identification of proposed active species, and some transient techniques, and the highest-ever CO_2-to-ethylene performance until then was achieved.

The type II interface with a suitable internal electric field imparts a lower recombination rate of photoinduced charge carriers and provides less transmission distance for charge transport. Notably, the photocatalytic capability of type II hybrid is directly determined by the terminal acceptors, which are often the semiconductors that possess a lower conduction band for photoreduction reaction while those with higher valence band levels for photooxidation reactions. $CuGaS_2/ZnS$ p–n type junction (a kind of type II junction), which was prepared via multistep cation exchange, was synthesized for photocatalytic H_2 evolution.[43] The intense charge space distributed in the p–n junction region situated at the atomic surface was unveiled as the key factor for the 15-fold H_2 evolution rate than that of pure $CuGaS_2$ under visible light.

Well-conduct carbon materials and some 2D materials are also developed to modulate the charge transport across the atomic interfaces. The $ZnS/CdIn_2S_4/rGO$ hierarchical arrays were reported to present a hydrogen generation rate of $6.82\ mmol\ g^{-1}$ h^{-1} by Yang et al., who designed an exemplary ternary hybrid with two kinds of intimate interfacial contact.[67] The properties of 2D materials are fully exploited for the epitaxial growth of ultrathin $CdIn_2S_4$ nanosheets over rGO, while the ZnS QDs were deposited in situ on the gap of $CdIn_2S_4$ arrays owing to the shared S lattice (Figure 9e). These two kinds of contact were formed jointly during one-step hydrothermal progress, indicating different joining mechanisms without competition. The intense contact facilitates the efficient migration of carriers between adjacent components and thus improves the charge separation efficiency. Moreover, the in situ interface of the two sulfides enables ZnS QDs to act as a terminal for electrons. Although it seems that the authors devoted skinny efforts to illustrating the formation of these intimate interfacial contacts, both the boosted hydrogen generation efficiency and the intuitive evidence of separate redox sites revealed the amended charge transport. Also, smooth charge transport and efficient charge separation were demonstrated at the interface of 2D–2D $MoS_2/$Cu-doped $ZnIn_2S_4$ (Cu–$ZnIn_2S_4$) mainly due to the large contact surface area in this unique 2D–2D structure.[68] In some cases, suitable band alignment and expected interface need the assistance of the interlayer. The original $ZnMoS_4/CuS$ p–n hybrid could not achieve the expected charge migration across the interface. For this regard, intercalated ZnO was introduced to contact both with $ZnMoS_4$ and CuS, inducing a suitable type II interfacial band bending for the kinetically favorable electron flow and efficient water splitting.[69]

4.1.2. Extension in Light Spectrum

The wide-spectrum light response remains a great challenge inhibiting practical photocatalytic deployments of solar

conversion. Introducing an atomic interface with a narrow bandgap light absorber or plasmonic nano-metals presents an available strategy to broaden light harvesting. The smooth charge exchange across the atomic interfaces is the precondition for the substantial extension of spectral response for binary absorber systems.

A complex CdS-based heterojunction of $Au@Pt/CdS/C_3N_4$ with plenty of 2D $Au/CdS/C_3N_4$ interfaces was designed and prepared to achieve an enhanced cumulative effect for visible-light-driven photocatalysis.[70] These interfaces were built via the electrostatic attraction assembly organization. In this report, light-harvesting capability was extended to 750 nm according to the observed UV–vis absorption spectrum mainly employing the LSPR effect of plasmonic Au (**Figure 10**a). Furthermore, Au–LSPR also boosted the charge transfer and charge separation across different atomic interfaces owing to the local electromagnetic field, resonance energy-transfer effect, and hot electron behaviors (Figure 10b–d). Eventually, the $Au@Pt/CdS/C_3N_4$ hetero-interface photocatalyst exhibited a 17.2-time and 14.3-time enhancement of H_2 evolution rate and CO_2 photoreduction rate than CdS/C_3N_4.

Narrow-band semiconductors could absorb wide-spectrum solar light themselves. Nevertheless, the narrow bandgaps often imply large carrier recombination probability,[71] which diminishes the significant rewards for spectrum response and direct application in photocatalysis. Atomic interfaces there contribute to the exciton dissociation and electron–hole pairs' separation. Generally, as mentioned before, the density of charges tends to rearrange owing to the interfacial interaction, which critically decides and describes the interfacial electric field.[72] The auxiliary interfacial electric field in the space charge layer provides an additional driving force for the maneuvering migration of the carriers, which facilitates charge separation and inhibits some possible charge recombination of hybrids.[73] In general terms, the increasing utilization of low-energy charge carriers, which are generated by absorbing long-wavelength light, also plays the purpose of broadening the light spectrum. This was exemplified in the work undertaken with the preparation of carbon quantum dots (CDs) decorated $MoSe_2$ for Cr(VI) reduction in the ultraviolet (UV)–visible–NIR region.[74] The interface of $MoSe_2/CDs$, which was established during a solvothermal procedure, displayed efficient charge transfer and light down-converting effect, achieving a Cr(VI) reduction rate of higher than 99%.

Special discussion on the extension of spectra is desired for the plasmonic copper chalcogenides. The vacancy concentration-dependent LSPR effect endows these chalcogenides with remarkable light absorption in the visible and NIR regions;[56a,59b,75] whereas, the effective utilization of the induced carriers is the key criterion for judging spectral broadening. A common challenge that existed is the collection predicament of their LSPR-driven hot charge carriers.[76] Configuring atomic semimetal interface or semi–semi interface with a robust interfacial electric field provides a paradigm to collect hot electrons or holes generated in plasmonic chalcogenides.[76a,77] A plasmonic construction of Cu_7S_4/Pd hybrid with an intimate semimetal interface was reported to present boosted sunlight utilization in the NIR range and the resulting enhanced catalytic performance for organic synthesis reactions.[60] Deficient Cu_7S_4 exhibited an LSPR character and harvested NIR light, and Pd served as an
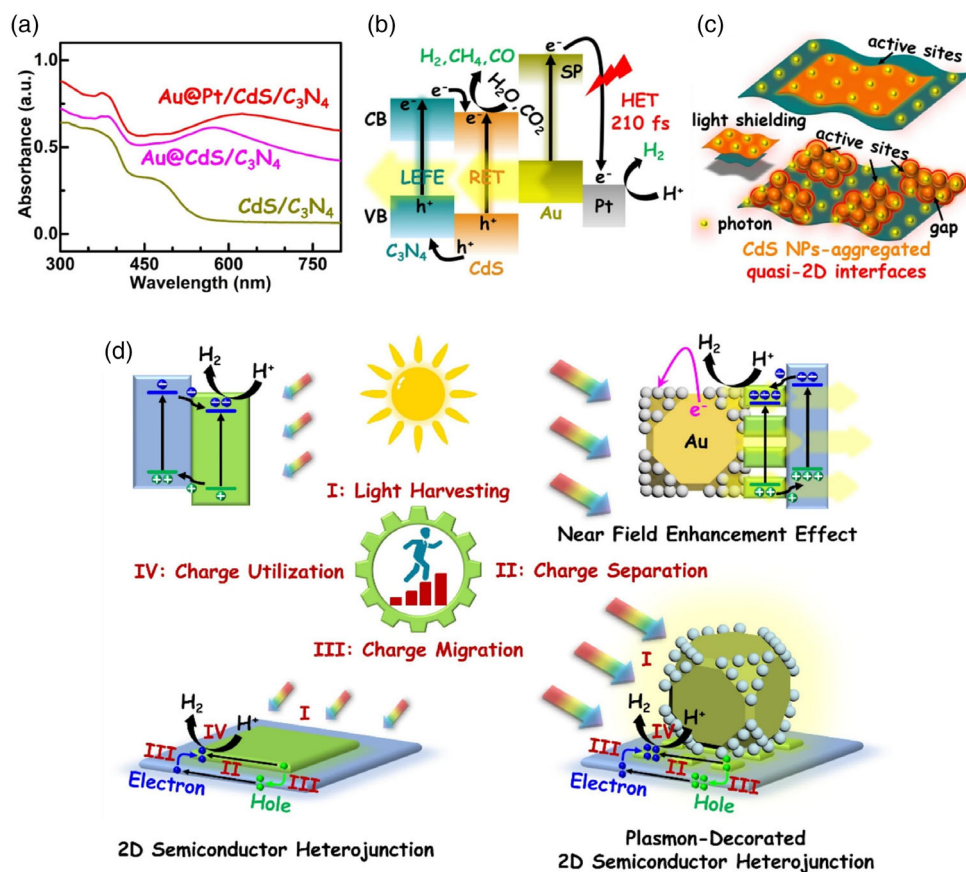
Figure 10. a) The UV–vis absorption of Au@Pt/CdS/C$_3$N$_4$ and other hybrids. b) The schematic illustration of the charge transport and c) the cumulative enhance mechanism of Au@Pt/CdS/C$_3$N$_4$ with plenty of atomic interfaces. d) Diagram depicting charge-carrier transfer in a 2D semiconductor heterojunction and a 2D semiconductor heterojunction decorated with plasmons. Reproduced with permission.[70] Copyright 2022, Elsevier.

engaging catalytic site. Favorable hot carrier transfer from plasmonic Cu$_7$S$_4$ to Pd enlarged the charge utilization and reduced the probability of charge recombination of the excited Cu$_7$S$_4$, more practically utilizing solar energy in the NIR region. In a previous CuS/Au self-assembled nanohybrid, effective resonance energy transfer, which absolutely depends on spectra overlap,[78] was observed at the interface as a key factor for the enhancement of rhodamine B (RhB) photodegradation.[30] Additionally, the near-field enhancement effect from both Au and CuS also made sense. It revealed that the well-wrapped CuS/Au interface built an effective channel for the synergistic LSPR characteristics. For a case of semi–semi interface mode, CuS injected hot holes to BiOCl to amplify its capability of light harvesting via a facet-modulated atomic interface, achieving enhanced NIR photocatalysis dominated by transversal LSPR mode.[76a]

4.1.3. Stability

It is widely concerned that the competitive reactivity and subsequent deactivation of the chalcogenides lattice hinder their long-term stability. Designing atomic interfaces was explored to play a role in stabilizing chalcogenides during the photocatalysis process. In a previous report, the coherent interface of CuGaS$_2$ and CdS was fabricated along with hybridization via in situ chemical precipitation.[79] The positive and directional electrons migration across the interface from nanocrystalline CdS to CuGaS$_2$ was claimed to be responsible for the inhibition of unfavorable Cu^{2+} formation, which is both the result of the Cu$^+$ self-corrosion and the reason for serious deactivation in CuGaS$_2$ (**Figure 11**a). This work presented the outstandingly amended activity (fourfold enhancement) and stability of photocatalytic CO$_2$ reduction for the production of CO by means of introducing the S coherent atomic interface. A novel CdS/TiO$_2$: Cu hollow structure was well designed for the application to simultaneously address CO$_2$ and H$_2$S syngas.[80] CdS was introduced on the surface of TiO$_2$: Cu spheres and filled the gap between TiO$_2$: Cu nanoparticles on the surface accompanied by highly dispersed atomic interfaces via an in situ hydrothermal etch-sulfurization approach. The atomic interfaces with robust contact were demonstrated to benefit the interfacial internal electric field and the efficient charge separation. This well-defined CdS/TiO$_2$: Cu hybrid behaved with a satisfactory synergistic photocatalysis output of CO$_2$ and H$_2$S with a CO yield of 781.3 μmol g^{-1} h^{-1} and a H$_2$ evolution rate of 5875.1 μmol g^{-1} h^{-1} simultaneously. In addition, the stability of this chalcogenide-based photocatalyst was protected by the remedial effects on S atoms and was displayed by the long-time photocatalytic test (Figure 11b,c). To
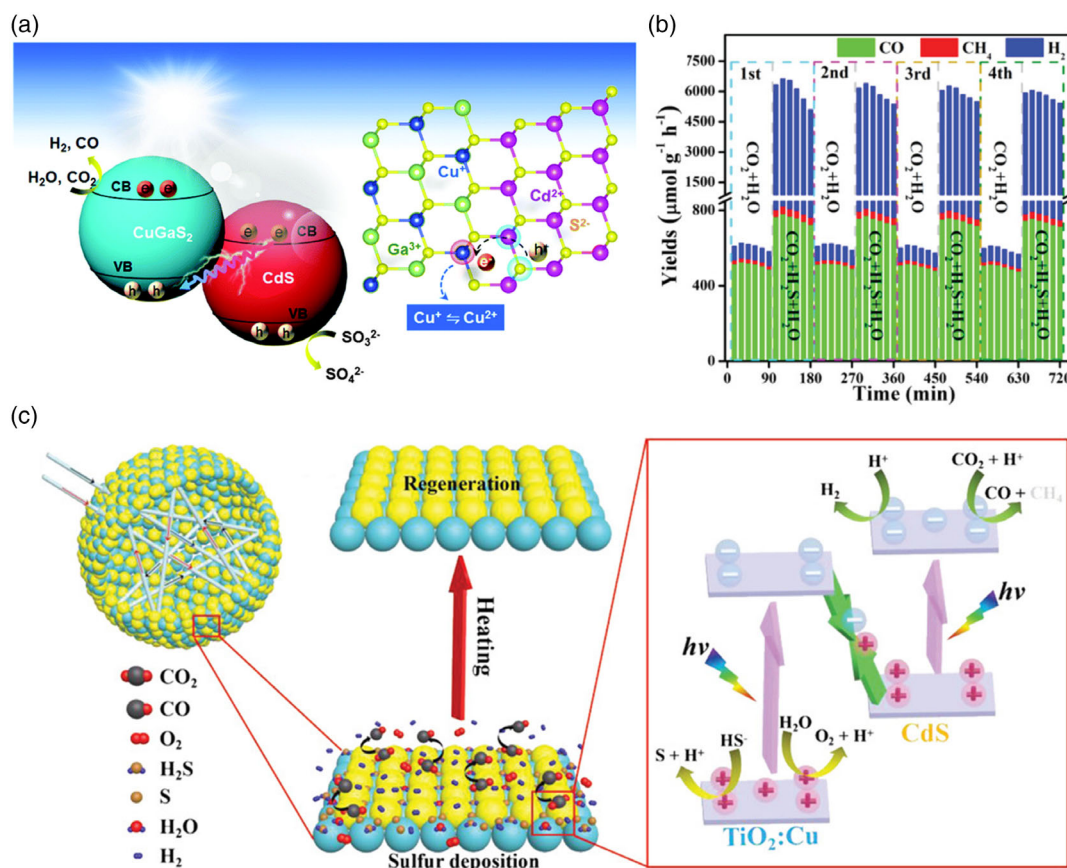
Figure 11. a) The proposed electron transfer and the benefit for surpassing Cu^{2+} formation. Reproduced with permission.[79] Copyright 2020, The Royal Society of Chemistry. b) Long-time stability tests for CdS/TiO_2: Cu in alternating cycles. c) The schematic diagram of the complex scattering of light, regeneration of the catalyst by heat-treatment desulfurization, and the charge-transfer route for CdS/TiO_2: Cu. Reproduced with permission.[80] Copyright 2022, Wiley-VCH.

advance the stability of CdS as well as alleviate charge recombination, an innovative design of CdS/CoP@AAH (amorphous aluminum hydroxide) was developed. The in situ phosphorization process assured an atomic interface between CdS and the co-catalyst. As expected, the amended architecture behaved with sufficient cycle stability and an enlarged output with an HER rate of $54.9\,mmol\,g^{-1}\,h^{-1}$ and an AQY of 40.62% at 450 nm.[81]

4.1.4. Optimal Integrated Effects

As we have been emphasizing, atomic interfaces provide a platform for accessing and regulating the various properties of hybrids, including optical, electrical, chemical, and physical properties. Correspondingly, photocatalytic processes, a technique that involves a variety of physical and chemical processes, also gain fruitful benefits through designing atomic interfaces. The atomic interfaces are mostly constructed for an integrated effect, reflecting a synergistic improvement in light harvesting, charge separation and transport, surface activity, and stability. The known complicated interactive correlation among these effects delivers a challenge to thoroughly distinguish them. But fortunately, most of the time, constructing a decent atomic

interface can usually take into account these vital criteria. These benefits, as mentioned before, are not usually quarantined as they coexist within a hybrid. More importantly, these integrated advantages are expected to bring hope for the practical application of photocatalysis.

Our group designed an ingenious ternary $Au@MoS_2/CdS$ hybrid with two kinds of atomic interfaces connected by Au–S bond and electrostatic interaction with shared S-lattice.[82] The investigation into the enhancement mechanism of the overall ameliorated HER performance revealed the integrated effects of interfacial charge transport. Under visible light illumination, both the injection of hot electrons excited in plasmonic Au nanorods to MoS_2–CdS interface and the directional charge migration from CdS to the MoS_2–CdS interface were guaranteed from the intimate contacts and small resistance (**Figure 12**a). On the one hand, the hot electron injection across the atomic interface provided the original energy for extending the light spectrum. Our work reported the first attempt to extend the light spectrum of CdS-based hybrids to the NIR region with a prominent AQY of >1% around 700 nm. On the other hand, these two atomic interfaces carried a kinetically conductive band alignment for efficient charge separation. Furthermore, the atomic interface of MoS_2–CdS was positioned as the HER active site owing to
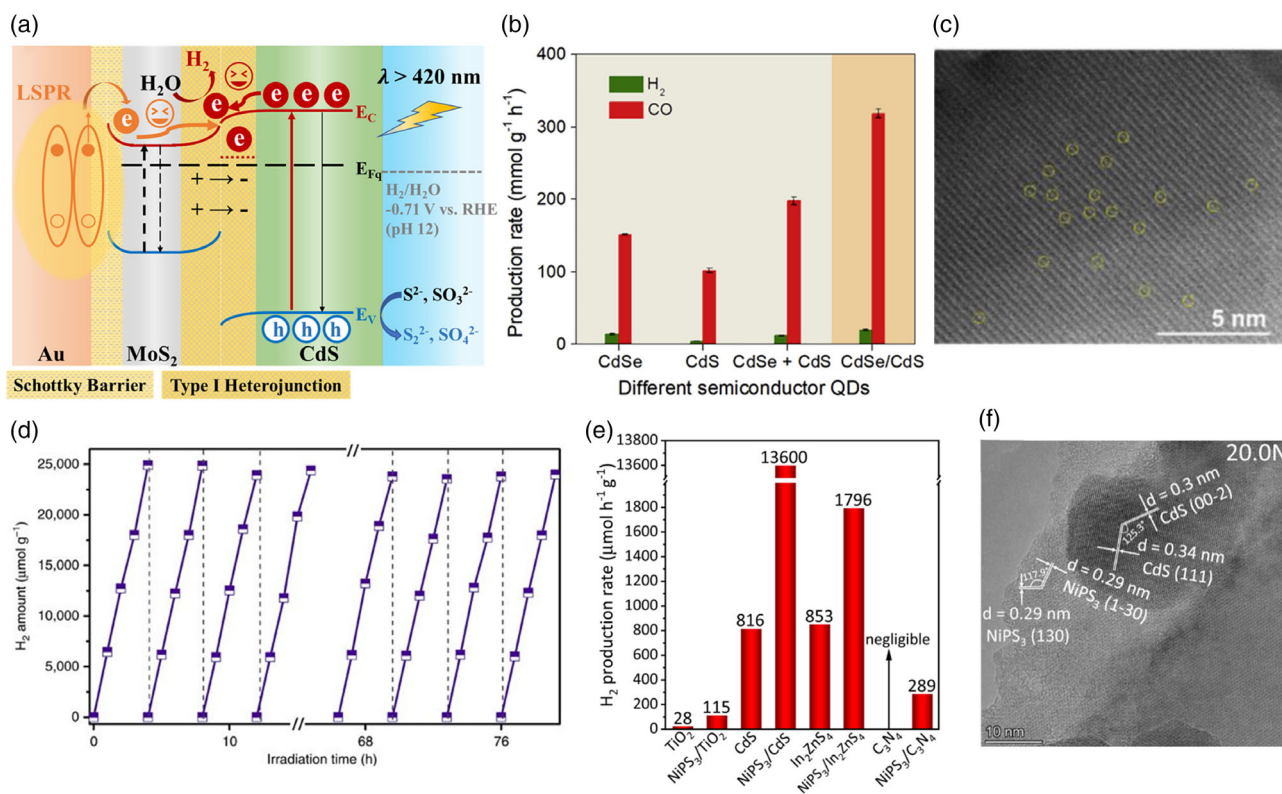
Figure 12. a) The proposed charge-transfer route across two kinds of atomic interfaces in the Au@MoS$_2$/CdS hybrid. Reproduced with permission.[82] Copyright 2023, Elsevier. b) The comparison of photocatalytic CO$_2$ reduction performance among CdSe/CdS hybrid with atomic interfaces, physical mixture of CdSe and CdS, single CdSe, and single CdS. Reproduced with permission.[83] Copyright 2019, Elsevier. c) HAADF–STEM image of CdS–Pd single atoms. Reproduced with permission.[92] Copyright 2022, American Chemical Society. d) Recycling photoactivity test of hetero-layered ZnIn$_2$S$_4$/MoSe$_2$. Reproduced with permission.[34] Copyright 2017, Springer Nature. e) The comparison of HER performance of different NiPS$_3$ hybrids, where NiPS$_3$/CdS presented superior efficiency. f) The HRTEM image of NiPS$_3$/CdS hybrid. Reproduced with permission.[97] Copyright 2022, Springer Nature.

the intermediate state from both experimental and theoretical viewpoints. Our work provides a vivid case for claiming the optimal integrated effects of designing atomic interfaces in boosting photocatalysis. In a comprehensive exploration carried out by Wu et al., CdSe/CdS QDs converted CO$_2$ into CO with a rate of ≈412.8 mmol g^{-1} h^{-1} and a selectivity of >96% accompanied by oxidative organic transformation.[83] The CdS shell was covered by applying a successive ion-layer adsorption and reaction method. The authors precisely controlled the thickness of the CdS shell to ≈3 atomic layers to architect a refined atomic interface. In addition, the physical mixture of CdSe and CdS was set as a comparison. It has been demonstrated that the CdSe/CdS hybrid with the intense atomic interface exhibited much superior photocatalytic performance than the simple physical mixture (Figure 12b). What emerges from these results is that CdS of atomic thickness dramatically enhanced the selectivity of pinacol production owing to the lower energy bottleneck of C–H cleavage. This work inspires that the refined regulation for the thickness of atomic interfaces is significant and is ingeniously influenced by the slow growth kinetics during the interfacial nucleation process. Similarly, the introduction of the atomic interface between In$_2$S$_3$ and CuInS$_2$ also contributed to an integrated influence for photocatalytic CO$_2$ reduction to CO. The report highlighted the roles of inhibiting charge recombination,

enhancing reactant absorption, and providing plentiful active sites.[45] Jiang et al. put their attention on the interface spatial engineering between CuS and g-C$_3$N$_4$ by altering the contact from the point, line, to face contact with diverse-dimensional growing CuS.[84] They demonstrated the superior advantages of face-to-face atomic interface for charge transfer and the face-to-face interfacial CuS/g-C$_3$N$_4$ hybrid displayed a 12-time improvement photocatalytic degradation apparent rate than pure g-C$_3$N$_4$. This work provided guidance for the investigation into the association between interface structure and photocatalytic performance from the insight into optical properties, electrical properties, and energy band levels. CuS is also combined with other semiconductors with relatively large bandgaps to comprehensively extend the overall photocatalytic output in the presence of interfacial interaction. CuS/ZnO hybrid was prepared to degrade methylene blue (MB), and it appeared that light harvesting, charge separation, catalytic activity, and recyclability of the hybrid were all advanced thanks to the synergistic effect of interfacial built-in electric field and the piezoelectric field of ZnO.[59a] Similarly, a Z-scheme CuS/ZnO was constructed to realize the coupling of piezo-catalysis and photocatalysis. The interfacial polarization electric field contributed to the dramatically amended degradation of tetracycline (TC).[85] Interfaces between CuS with BaTiO$_3$ and even insulator BaSO$_4$ and CuSe with

$CaCO_3$ also made a difference for the enlarged photocatalytic feedbacks, which is ascribed to the suitable band alignment and efficient interfacial electric field.[86]

4.2. Chalcogenides as Supports of Single Atoms

Parallel to the discovery of single atoms and the exploration of their unique characteristics, concerns were expressed about uniformly dispersing single atoms and rationally controlling their states of anchoring. The merits of high surface-to-volume and the unique electric properties render 2D chalcogenides (especially TMDs like MoS_2) practical supports to disperse single atoms. It can be presumed that atomic interfaces with intense bonds between single atoms and their supports make a great difference in charge modulation and catalysts productivity.

Tsang et al. incorporated isolated Co atoms into the basal planes of MoS_2 single-layer sheets for dramatically enhanced catalytic properties for hydrodeoxygenation (HDO).[87] The Co-MoS_2 atomic interface was formed benefiting from the intense covalent bond of Co–S–Mo. A large number of sulfur vacancies are promoted proximal to the doped Co atoms, and the strong immobilization between basal planes of MoS_2 and Co atoms is also attributed to the interaction of Co's d-orbitals with Mo. Compared with conventionally prepared samples, the Co-MoS_2 hybrid with atomic interface exhibited superior photocatalysis capability and stability for the HDO of 4-methylphenol to toluene with reduced reaction temperature from 300 to 180 °C. The Co–S–Mo interfacial sites were ascribed as the key factor for these dramatically enhanced behaviors. Another work dispersed Mo into MoS_2 to verify the activity of catalysts containing solely Mo for efficient hydrodesulfurization (HDS).[88] Controllable CO_2 reduction catalysts were developed and selected with the method of first-principles calculations by incorporating isolated transition-metal atoms (Ni, Pd, Rh, Nb, Zr, and Re) into In_2Se_3 monolayer, which demonstrated to be excellently regulated via ferroelectric swapping by adjusting the d-band center and occupying the anchored metal atoms.[89] By the comprehensive screen for CO_2 reduction catalysts with sound efficiencies and selectivity, the significant promise for 2D ferroelectric chalcogenides materials as the supports of single atoms has been identified. An attachment of Au single atoms to monolayer MoS_2 was reported by utilizing a spontaneous defect-free functionalization method.[90] The interfacial S–Au–Cl coordination played a key role in charge transport and tuning the electric properties of MoS_2 as well as heat dissipation. This Au-loaded MoS_2 with 1H phase was expected to be a candidate device for catalysis. The 2D MoS_2 was synthesized as the support of Ru single atoms for H_2 evolution.[91] What is interesting about this architecture is that the intimate interaction at Ru/MoS_2 interface sparked the phase transition and S vacancies in MoS_2, which dramatically tailored the electronic structure and HER performance.

CdS was selected as both the main absorber and the support of single Pd atoms thanks to the Pd–S_x sites (Figure 12c).[92] The atomic surface with in situ coordination served as satisfactory hydrogen-transfer shuttles and thus endowed photoinduced electrons with a longer lifetime. The interfacial Pd–S_x species contributed to the necessary hydrogenation process and the subsequent generation of the secondary amine N-benzylaniline. Moreover, the Pd/CdS hybrid with the atomic interface expressed good adaptability to different alcohols and amines.

4.3. Chalcogenides as Co-Catalysts

Atomic interfaces sometimes behave as absorption sites, mainly facilitating the adsorption of reaction intermediates and other surface reactions. As a result of the optimized adsorption energy of intermediates, the rate-determining step can be carried out at a faster rate. The intrinsic contribution origins from the different coordination environments. This effect occurs especially in the presence of co-catalysts. Transition-metals-based chalcogenides (M–VI, M for Mo, Ni, Co, Cu, Fe, etc.; VI for S, Se, Te) with low electrical resistivity, variable valence states of metal elements, and exposed active sites have obtained a great deal of attention as co-catalysts for HER or other photocatalytic applications.[93] Their crystal structures have been reviewed in previous work[38a]; thus we here do not place our focus on the summarization of structures but on their growth across the surface and their benefits for photocatalysis.

The interfaces of the $ZnIn_2S_4$/$MoSe_2$ hybrid were constructed in multiple efforts with different focuses. Being reviewed in Section 4.1.1, $ZnIn_2S_4$/$MoSe_2$ was prepared to demonstrate the significance of interfacial Mo–S bonds as the bridge for charge transport via a Z-scheme mechanism.[41] Differently, in an early investigation, the strategy to obtain an atomically thin few-layers hybrid was underlined. $ZnIn_2S_4$ was exfoliated into a single-unit-cell layer structure after a self-surface charge exfoliation.[34] Few-layered $MoSe_2$ was then attracted and assembled onto the surface of $ZnIn_2S_4$ serving as the co-catalyst via the electrostatic coupling. Owing to the atomic thickness of the controlled interface, the subsequent efficient charge transfer across the interface was guaranteed. Consequently, the design in this work produced a prominent hydrogen evolution capability of $6454\,\mu mol\,g^{-1}\,h^{-1}$ as well as robust stability with prolonged 80 h cycling showing negligible activity loss (Figure 12d). In another report, the $ZnIn_2S_4$/$MoSe_2$ interface served for electron storage and more active sites with a photocatalytic H_2 rate of $2228\,\mu mol\,g^{-1}\,h^{-1}$.[94] MoS_2 and MoO_2 were anchored on CdS hollow spheres as dual cocatalyst for bifunctional photocatalytic H_2 production coupled with pyruvic acid (PA) generation.[95] MoS_2 as the electron acceptor of photogenerated electrons in CdS promoted the HER capability due to the close contact and low transport resistance across the interface.

CoS clusters nucleated in situ at the surface of CdS nanorods as the co-catalyst, along with the construction of atomic interface linked by Cd–S–Co bonds. The charge rearrangement at this interface was demonstrated to benefit the modulation of the d-band center and the improvement of charge separation via reducing thermodynamic energy barriers at the interface. With no doubt, the CoS/CdS hybrid presented a high H_2 evolution rate of $65.7\,mmol\,g^{-1}\,h^{-1}$ with the aid of active sites at the interfaces.[96] $NiPS_3$ was chosen as the co-catalyst for solar-driven H_2 evolution while the interface of $NiPS_3$/CdS was extruded in the HER performance by comparing it with other semiconductors (Figure 12e). As for the reason, this combination expressed the most intimate correlated interface (Figure 12f), which attributed to the sufficient carrier dissociation and transport. Furthermore, both the abundant edge P/S sites across the interface and S sites on co-catalyst $NiPS_3$ advanced the photocatalytic HER output, where an HER rate of $13.6\,mmol\,g^{-1}\,h^{-1}$ was

achieved.[97] With a view to the activity of Ni_3S_4 for assistance in water oxidation, an atomic interface of CdS/Ni_3S_4 was built and was applied to enlarge the photocatalytic outcome of H_2 evolution as well as H_2O_2 production, respectively.[98] The interfacial tense Re–O covalent bond occupied the atomic interface of $BaTiO_3@ReS_2$ and exhibited an electron transport channel with reduced resistance. The co-catalyst ReS_2 with a metal phase accepted the photoinduced electrons from the piezoelectric $BaTiO_3$ and enhanced the activity for superoxide radicals benefiting photocatalytic degradation.[99] CuS was illustrated to be a satisfactory alternative to the noble-metal cocatalysts for visible-driven H_2 evolution in a previous hybrid comprising CuS/CdS.[100] With an in situ formed interface, CuS/CdS exhibited more efficient charge transfer across the interface and electron–hole separation, achieving a H_2 generation rate of twice the CdS/Pt hybrid.

5. Advanced Characterization for Atomic Interfaces

The rapid and sustainable development of nanoscience has triggered the extensive investigation of structures, properties, and changes in nanoscales. The frequent use of a suite of in situ and ex situ characterization approaches provide intuitive evidence for the structural and chemical information of nanomaterials through electron microscope imaging, energy and wave spectroscopic, electrochemistry, physical performance test, thermal analysis, and other diverse aspects. Specific to the investigation of an atomic interface, all of its four building blocks (components, morphology, chemical environment, and stability) can be represented and explored directly or indirectly by carrying out these characterizations. From the perspective of atomic interfaces served for boosting photocatalysis, structure, binding information, interfacial impedance, and the inherent photocatalytic enhancement mechanism (including charge-transport route, active sites, and stability) of atomic interfaces desire to be comprehensively comprehended by using diverse advanced characterizations shown in **Figure 13**.

The insight into interfaces' structures and morphologies could be provided by the atomic-level microscopic tactic. High-resolution scanning transmission electron microscopy (STEM) supplies intuitive atomic distribution. Similarly, HAADF–STEM mode usually could give an atomic arrangement that cannot be clearly observed under a bright field.[101] The atomic interfaces of ZnSe/ZnS were visually observed and presented in the HAADF–STEM images (**Figure 14**a–e).[50] The atomic structure and the defects of TaS_2 were intuitively obtained by HAADF–STEM seen in Figure 14f,g.[102] The atomic interface of the CdS/MoS_2 hybrid was observed with HAADF and annular bright-field (ABF) STEM images in Figure 4a.

Advanced characterization methods serve to observe the interfaces on the one hand, and on the other hand, need to give bonding information. A variety of spectral and energy spectrum analyses can be carried out to address this demand. From the (in situ) characterization of XPS, the intense chemical bonds could be revealed by the shift of binding energy. XPS peaks intensity variation and the new peak formation also indicate the potential chemical bonds. EPR shows the presence of vacancy defects and unpaired electrons, which are the prerequisites for the architecture of atomic interfaces in some cases. In the same way,
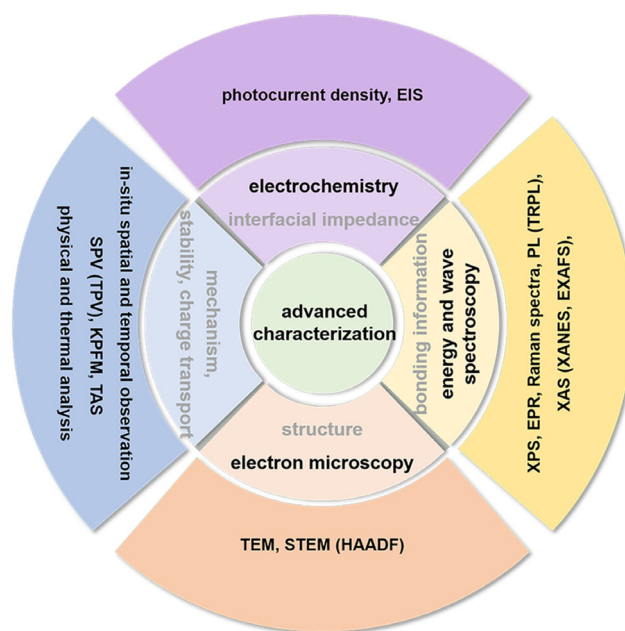

Figure 13. The involved advanced characterization for the investigation into atomic interfaces served for boosting photocatalysis.

Raman spectra also provide information on atomic bonds since the vibration is sensitive to the local environment. The bonding state of the interface of $MoS_2/SnS_2/rGO$ was observed from the Raman analysis listed in Figure 14h.[36] Upon introducing hybridization interfaces, the instinct lattice vibration of SnS_2 redshifted owing to the insertion of Mo^{4+}, while a redshift also occurred in the A_{1g} mode of MoS_2 due to the local lattice spacing mismatch at the interface. Moreover, a defect-induced band and a symmetrically allowed band were also observed. These messages demonstrated the chemical bonds across the as-formed atomic interfaces. Defects in MoS_2 were also confirmed by peak shifts in Raman spectra and intensity decrease in photoluminescence (PL) spectra.[103]

Ingenious PL spectroscopy probes discrete energy levels as well as the structural composition of photocatalyst hybrids in a nondestructive manner.[104] Trapping sites along with electron–hole pairs segregation and migration will also be illustrated with the assistance of the PL technique. To systematically investigate the electronic structures and coordination environments of the as-prepared defects-induced hybrid and the formed atomic interface, X-ray absorption spectroscopy (XAS) analyses including X-ray absorption near-edge structure (XANES) and the extended X-ray absorption fine structure (EXAFS) are usually performed.[105] The lattice distortion located at the SnS_2/SnO_2 interfaces was reflected by XANES measurement of the Sn K-edge. From Figure 14i, the intensities of Sn–O and Sn–S bonds changed with the sulphuration time, and the extent of the Sn–Sn bond after interfaces were built was also reflected in the slight shift toward the R direction of the Sn–Sn peak.[52]

Electrochemical methods provide a visual perspective to measure macroscopically low contact resistance at atomic-scale interfaces. The photocurrent density helps to determine carrier

ADVANCED
SCIENCE NEWS
www.advancedsciencenews.com

Solar
RRL
www.solar-rrl.com
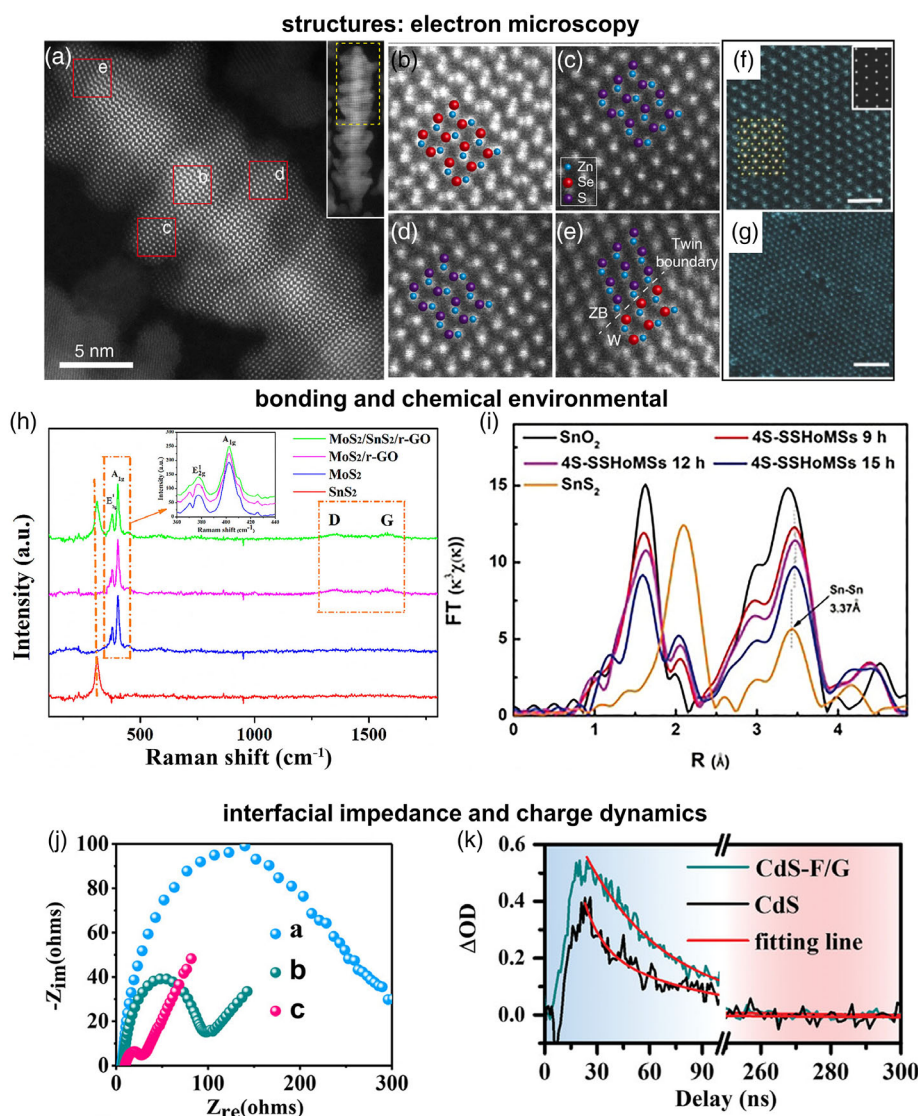
Figure 14. a) HAADF–STEM images of ZnSe/ZnS core–shell hybrid. b–e) Zoom in observation of areas indicated in image (a), where Zn atoms are marked in blue, Se atoms in red, and S atoms in purple. Reproduced with permission.[50] Copyright 2019, Springer Nature. High-resolution HAADF–STEM images of f) pristine and g) plasma-treated defective TaS$_2$ nanosheets, respectively. Reproduced with permission.[102] Copyright 2016, Wiley-VCH. h) Raman spectra of MoS$_2$/SnS$_2$/rGO hybrid with multi-interfaces and changes in Raman bands. Reproduced with permission.[36] Copyright 2019, American Chemical Society. i) Fourier-transformed magnitudes of Sn K-edge extended X-ray absorption fine structure (EXAFS) spectra of quadruple-shelled SnS$_2$–SnO$_2$ compared with SnO$_2$. Reproduced with permission.[52] Copyright 2020, Wiley-VCH. j) Electrochemical impedance spectroscopy (EIS) Nyquist spectra of ZnIn$_2$S$_4$/MoS$_2$ ([c] in the picture) photocatalyst hybrid and the comparison with bulk ZnIn$_2$S$_4$ and ZnIn$_2$S$_4$ with S vacancies ([a] and [b] in the picture, respectively). Reproduced with permission.[42] Copyright 2018, American Chemical Society. k) Transient absorption spectroscopy (TAS) (on nanosecond timescale) decay kinetics of CdS and CdS-fullerene/graphene hybrid. Reproduced with permission.[109] Copyright 2022, Wiley-VCH.

utilization, and the electrochemical impedance spectroscopy (EIS) diagram visually shows the impact of carrier migration on the interfaces. Pei et al. investigated the charge-transfer performance across interfaces of ZnIn$_2$S$_4$/MoS$_2$ with S vacancies in ZnIn$_2$S$_4$ and interfacial S-metal bonds via EIS spectra.[42] As shown in Figure 14j, hybrid with defects-induced atomic interfaces showed the smallest Nyquist radius, indicating the smallest transportation resistance along the interface.

In addition, the role and enhancement mechanism of atomic-level interfaces in photocatalysis should also be obtained. For this

matter, characterizations with spatial and temporal resolutions undergo noteworthy improvements and play a more and more essential role in the field of photocatalysis. The quest for further apprehending the charge dynamics has stimulated the rise of specifically adapted and parallelized characterization techniques.[106] The steady surface photovoltage spectroscopy (SPV) and its transient photovoltage spectroscopy technique (TPV) visualize the separation of photogenerated charge carriers. Our group observed a considerably more positive surface voltage in Au@MoS$_2$/CdS than CdS from the SPV spectra, indicating more

holes left at the surface of CdS and a vivid contribution of the atomic interfaces for charge separation.[82] Kelvin probe force microscopy (KPFM), one of the modes of atomic force microscope (AFM), also provides a channel to detect the charge-carrier dynamics.[107] Shi et al. disclosed the mediated charge-sinking effect of carbon dots at the atomic interfaces with Cu–In–Zn–S and the actives sites exposed by MoS$_2$ by comparing a series of TPV signals.[108] Transient absorption spectroscopy (TAS) is gradually well known for its ability to monitor carrier behavior on different time scales under irradiation and dark conditions. The decay kinetics of charge recombination and transition to the ground state in the CdS–fullerene/graphene hybrid was identified via the TAS technique on a nanosecond timescale (Figure 14k).[109] The interfacial electron transfer ($\approx$30.3 ps) and the sub-microsecond-lived excited states ($\approx$172.6 ns) were revealed. This work provided a suitable example for displaying the optimized electronic structure associated with interfacial electron and hole transfer for promoted photocatalysis.

Feedback from these in situ characterizations helps guide accelerated optimization on the design of the atomic interface. Academician Li Can and coworkers tracked the charge-transfer process in a single Cu$_2$O particle and depicted the holistic carrier migration on the femtosecond to second timescale by performing spatiotemporally resolved surface photovoltage measurements.[106] This is a huge progress toward the further illustrating underlying mechanism of other photocatalytic systems and it presents hope for an investigation into interfacial charge behaviors. Hopefully, the charge carriers' behavior and even the formation mechanism of the atomic interfaces could also be cast light on via the progressively advanced characterizations.

6. Summaries and Outlooks

Materials science research on interfaces has reached an unprecedented level and will remain an important topic for years to come. Particularly, significant attention has been invested in simultaneously amending the properties of interfaces in photocatalyst hybrids for their decisive role in charge behaviors. Atomic interfaces build a bridge and hold the prospect for expected charge flow to access rational optimization of optical, electrical, chemical, and physical properties of hybrids and lay the foundations for more extensive photocatalytic applications. This essay sets out to pursue a comprehensive understanding of the association between designing atomic interfaces in chalcogenides and maneuvered photocatalytic output. The fundamentals and potentials of atomic interfaces for boosting photocatalysis have been concisely illustrated in this review, followed by the formation strategies of atomic interfaces in chalcogenides. Weak force (electrostatic attraction and van der Waals force)–driven interaction, defects-induced chemical bond, cation exchange, and slow epitaxy are concluded as four feasible approaches to fabricate atomic interfaces in chalcogenides, in which intense atomic bonds are underlined. Afterward, the diverse benefits of atomic interfaces for ameliorated photocatalytic capability are concluded by summarizing research progress about advanced atomic interfaces of chalcogenides for boosting photocatalysis. When chalcogenides play a different role in photocatalyst hybrids, the atomic interfaces tend to exhibit different

functions. The optimal atomic interfaces with predominant chalcogenides photocatalysts or co-catalysts have been demonstrated to play a pivotal role in regulating light harvesting, accelerating charge separation, directing carriers' migration, enriching active reaction centers, and even inhibiting instability. The identity of the single atom's support of chalcogenides means a multifunctional atomic interface. Together these efforts and expositions provide essential insights into the roles of atomic interfaces for enlarged photocatalysis outcomes. At last, the advanced characterizations of atomic interfaces are introduced with pioneering cases. Characterization, including electron microscopy, energy and wave spectroscopic, electrochemistry method, in situ observation with spatial and temporal resolutions, physical performance test, thermal analysis, and other diverse aspects, provides a plentiful vision to explore the atomic interfaces.

Despite current encouraging efforts of designing atomic interfaces in chalcogenides, certain challenges still remain surrounding the fabrication techniques of atomic interfaces, the design principles in a predictable manner, the identification of underlying mechanisms, and the judging criteria of the synergistic effect of the atomic interfaces for photocatalytic applications. Therefore, we put forward the challenges and prospects from the following aspects. 1) To advance the current state of the art in the configuration of hybrid, increasing strenuous endeavors should be directed toward grasping how to controllably target interfaces with intense contact and stability. It takes suitable atomic interfaces to really make a difference for photocatalysis since excessive interfaces will form reassembly centers and thus cause the recombination of excited carriers as well as hinder light absorption. The approach to forming an interface in chalcogenides is a decisive factor. We call for the removal of simple physical or random mixtures, which are unstable and ineffective in the long run. Even the interfaces devised by weak interaction also suffer from underlying cleavability. Defects-induced chemical bonds, cation exchange, and slow epitaxy are continuously desired to architect atomic interfaces in chalcogenides. Other novel and maneuverable strategies that fully consider the characteristics of chalcogenides and interface combinations are still urgently required in the future. 2) The formation mechanism of some multinary chalcogenides and interfacial nucleation remains unclear, which poses a theoretical obstacle to the further controllable construction of atomic-level interfaces. Great efforts still need to endeavor toward the crystallization process of multinary chalcogenides. Recent high-entropy effects, lattice distortion effect, sluggish diffusion effect, and "cocktail" effect in multinary chalcogenides provide a variety of visions for this challenge.[18c,110] These findings raise important theoretical issues that have a bearing not only on crystallization but also on interfacial nucleation. An in-depth insight into the behavior of the interface during interfacial nucleation is also crucial to assess the performance of the photocatalysis device. Interfacial nucleation is greatly affected by temperature and concentration of precursor. However, high-temperature conditions sometimes even destroy the primary chemical bonds or structures present in each phase. The deeper nucleation mechanism both in bulk and interface needs to be proposed to solve the aforementioned obstructions from the theoretical level. 3) The DFT calculations of interface chemical bonds could provide a high-throughput screening for available atomic interfaces. It is still challenging to establish a rigorous correlation between the chemical

environment and photocatalysis active sites. The adsorption energies of various reactants and intermediates as well as the desorption of intermediate and final products could be quantified via certain theoretical calculations to guide this dependence. In addition, the electric behavior at the atomic interfaces, including the density of states (DOS) and energy band structures, is coveted to be cast light on through some theoretical calculations. 4) Further research is required to better comprehend the complex linkages between atomic interfaces and the resulting modulation in photocatalytic performance. The development of temporally resolved analytic techniques, adapted to capture carrier dynamics, remains a key task to achieve an understanding of important factors affecting the unambiguous photocatalysis process. At present, the encouraging maps of electron and hole migrations during the photocatalysis process in accordance with changes in surface voltages in real time have been drawn. However, obviously, current detection raises high requirements for crystal crystallinity and grain size, and the observation at the atomic level needs further technical progress. In situ integral characterization techniques with high spatial and temporal resolution will be a powerful channel to reveal the carrier behaviors and photocatalytic reaction mechanism in the future.

Conflict of Interest

The authors declare no conflict of interest.

[1] a) Z. Wang, K. Gao, Y. Kan, M. Zhang, C. Qiu, L. Zhu, Z. Zhao, X. Peng, W. Feng, Z. Qian, X. Gu, A. K. Jen, B. Z. Tang, Y. Cao, Y. Zhang, F. Liu, *Nat. Commun.* **2021**, *12*, 332; b) J. Fu, Z. Fan, M. Nakabayashi, H. Ju, N. Pastukhova, Y. Xiao, C. Feng, N. Shibata, K. Domen, Y. Li, *Nat. Commun.* **2022**, *13*, 729; c) J. Ma, G. Yang, M. Qin, X. Zheng, H. Lei, C. Chen, Z. Chen, Y. Guo, H. Han, X. Zhao, G. Fang, *Adv. Sci.* **2017**, *4*, 1700031; d) Q. Dong, C. Zhu, M. Chen, C. Jiang, J. Guo, Y. Feng, Z. Dai, S. K. Yadavalli, M. Hu, X. Cao, Y. Li, Y. Huang, Z. Liu, Y. Shi, L. Wang, N. P. Padture, Y. Zhou, *Nat. Commun.* **2021**, *12*, 973.

[2] a) Y. Zhang, P. Lei, X. Zhu, Y. Zhang, *Nat. Commun.* **2021**, *12*, 6178; b) Z. Li, J. Wei, F. Wang, Y. Tang, A. Li, Y. Guo, P. Huang, S. Brovelli, H. Shen, H. Li, *Adv. Energy Mater.* **2021**, *11*, 2101693; c) J. Li, L. Zhang, Z. Chu, C. Dong, J. Jiang, Z. Yin, J. You, W. Lan, X. Zhang, *Adv. Opt. Mater.* **2022**, *10*, 2102563.

[3] a) X. Miao, S. Guan, C. Ma, L. Li, C. W. Nan, *Adv. Mater.* **2022**, 2206402, https://doi.org/10.1002/adma.202206402; b) S. Li, S. Luo, L. Rong, L. Wang, Z. Xi, Y. Liu, Y. Zhou, Z. Wan, X. Kong, *Molecules* **2022**, *27*, 3989.

[4] a) S. Zou, B. Lou, K. Yang, W. Yuan, C. Zhu, Y. Zhu, Y. Du, L. Lu, J. Liu, W. Huang, B. Yang, Z. Gong, Y. Cui, Y. Wang, L. Ma, J. Ma, Z. Jiang, L. Xiao, J. Fan, *Nat. Commun.* **2021**, *12*, 5770; b) L. Liu, S. Wang, H. Huang, Y. Zhang, T. Ma, *Nano Energy* **2020**, *75*, 104959.

[5] H. I. Un, J. Y. Wang, J. Pei, *Adv. Sci.* **2019**, *6*, 1900375.

[6] S. Bai, N. Zhang, C. Gao, Y. Xiong, *Nano Energy* **2018**, *53*, 296.

[7] S. Zhang, Y. Si, B. Li, L. Yang, W. Dai, S. Luo, *Small* **2021**, *17*, 2004980.

[8] M. Ma, Y. Huang, J. Liu, K. Liu, Z. Wang, C. Zhao, S. Qu, Z. Wang, *J. Semicond.* **2020**, *41*, 091702.

[9] Z. Chen, X. Li, C. Yang, K. Cheng, T. Tan, Y. Lv, Y. Liu, *Adv. Sci.* **2021**, *8*, 2101883.

[10] J. Liu, H. Zhao, Z. Wang, T. Hannappel, U. I. Kramm, B. J. M. Etzold, Y. Lei, *Sol. RRL* **2022**, *6*, 2200181.

[11] a) I. M. F. Tanimoto, B. Cressiot, S. J. Greive, B. Le Pioufle, L. Bacri, J. Pelta, *Nano Res.* **2022**, *15*, 9906; b) M. K. Samantaray, E. Pump, A. Bendjeriou-Sedjerari, V. D'Elia, J. D. A. Pelletier, M. Guidotti, R. Psaro, J.-M. Basset, *Chem. Soc. Rev.* **2018**, *47*, 8403; c) W. Wang, Y. Shi, C. Zhang, S. Hong, L. Shi, J. Chang, R. Li, Y. Jin, C. Ong, S. Zhuo, P. Wang, *Nat. Commun.* **2019**, *10*, 3012; d) F. A. Chowdhury, M. L. Trudeau, H. Guo, Z. Mi, *Nat. Commun.* **2018**, *9*, 1707; e) X. Jiang, X. Nie, X. Guo, C. Song, J. G. Chen, *Chem. Rev.* **2020**, *120*, 7984; f) C. Dong, Y. Yang, X. Hu, Y. Cho, G. Jang, Y. Ao, L. Wang, J. Shen, J. H. Park, K. Zhang, *Nat. Commun.* **2022**, *13*, 4982.

[12] a) T. H. Gu, X. Jin, S. J. Park, M. G. Kim, S. J. Hwang, *Adv. Sci.* **2021**, *8*, 2004530; b) C. Pan, Z. Mao, X. Yuan, H. Zhang, L. Mei, X. Ji, *Adv. Sci.* **2022**, *9*, 2105747; c) S. Das, J. Pérez-Ramírez, J. Gong, N. Dewangan, K. Hidajat, B. C. Gates, S. Kawi, *Chem. Soc. Rev.* **2020**, *49*, 2937.

[13] X. Ma, Y. Wei, Z. Wei, H. He, C. Huang, Y. Zhu, *J. Colloid Interface Sci.* **2017**, *508*, 274.

[14] a) X. Periole, A. M. Knepp, T. P. Sakmar, S. J. Marrink, T. Huber, *J. Am. Chem. Soc.* **2012**, *134*, 10959; b) M. Sakamoto, T. Kawawaki, M. Kimura, T. Yoshinaga, J. J. M. Vequizo, H. Matsunaga, C. S. K. Ranasinghe, A. Yamakata, H. Matsuzaki, A. Furube, T. Teranishi, *Nat. Commun.* **2019**, *10*, 406.

[15] a) M.-R. Gao, Y.-F. Xu, J. Jiang, S.-H. Yu, *Chem. Soc. Rev.* **2013**, *42*, 2986; b) Y. Yang, K. Wang, H. W. Liang, G. Q. Liu, M. Feng, L. Xu, J. W. Liu, J. L. Wang, S. H. Yu, *Sci. Adv.* **2015**, *1*, 1500714; c) S. Adabala, D. P. Dutta, *J. Environ. Chem. Eng.* **2022**, *10*, 107763.

[16] S. Song, J. Qu, P. Han, M. J. Hülsey, G. Zhang, Y. Wang, S. Wang, D. Chen, J. Lu, N. Yan, *Nat. Commun.* **2020**, *11*, 4899.

[17] a) H. Fu, A. Tang, *J. Semicond.* **2020**, *41*, 091706; b) S. Kerour, A. Bouloufa, M. Lasladj, K. Djessas, K. Medjnoun, *J. Semicond.* **2021**, *42*, 072701; c) Z. Yin, M. Hu, J. Liu, H. Fu, Z. Wang, A. Tang, *J. Semicond.* **2022**, *43*, 032701.

[18] a) H. Li, C. Tsai, A. L. Koh, L. Cai, A. W. Contryman, A. H. Fragapane, J. Zhao, H. S. Han, H. C. Manoharan, F. Abild-Pedersen, J. K. Nørskov, X. Zheng, *Nat. Mater.* **2016**, *15*, 48; b) A. Gautam, S. Sk, U. Pal, *Phys. Chem. Chem. Phys.* **2022**, *24*, 20638; c) L. Wu, J. P. Hofmann, *Curr. Opin. Electrochem.* **2022**, *34*, 101010.

[19] a) L. Zhang, Z.-J. Zhao, T. Wang, J. Gong, *Chem. Soc. Rev.* **2018**, *47*, 5423; b) J. H. Han, M. Kwak, Y. Kim, J. Cheon, *Chem. Rev.* **2018**, *118*, 6151; c) N. K. Oh, C. Kim, J. Lee, O. Kwon, Y. Choi, G. Y. Jung, H. Y. Lim, S. K. Kwak, G. Kim, H. Park, *Nat. Commun.* **2019**, *10*, 1723.

[20] H. Zhong, Y. Feng, N. Alonso-Vante, *Curr. Opin. Electrochem.* **2022**, *34*, 101016.

[21] a) Z. Zhao, M. Lu, Z. Mao, J. Xiao, Q. Huang, X. Lin, Y. Cao, *Int. J. Biol. Macromol.* **2020**, *152*, 223; b) X. Chen, C. Li, M. Grätzel, R. Kostecki, S. S. Mao, *Chem. Soc. Rev.* **2012**, *41*, 7909.

[22] a) P. Raizada, V. Soni, A. Kumar, P. Singh, A. A. Parwaz Khan, A. M. Asiri, V. K. Thakur, V.-H. Nguyen, *J. Materiomics* **2021**, *7*, 388; b) C. Li, J. Li, Y. Huang, J. Liu, M. Ma, K. Liu, C. Zhao, Z. Wang, S. Qu, L. Zhang, H. Han, W. Deng, Z. Wang, *J. Semicond.* **2022**, *43*, 021701; c) Y. Xiao, M. Zhou, M. Zeng, L. Fu, *Adv. Sci.* **2019**, *6*, 1801501.

[23] N. Serpone, A. V. Emeline, V. K. Ryabchuk, V. N. Kuznetsov, Y. M. Artem'ev, S. Horikoshi, *ACS Energy Lett.* **2016**, *1*, 931.

[24] M. Qiao, J. Liu, Y. Wang, Y. Li, Z. Chen, *J. Am. Chem. Soc.* **2018**, *140*, 12256.

[25] C. F. Tan, W. L. Ong, G. W. Ho, *ACS Nano* **2015**, *9*, 7661.

[26] X. Zhao, J. Feng, J. Liu, J. Lu, W. Shi, G. Yang, G. Wang, P. Feng, P. Cheng, *Adv. Sci.* **2018**, *5*, 1700590.

[27] C. Q. Li, X. Du, S. Jiang, Y. Liu, Z. L. Niu, Z. Y. Liu, S. S. Yi, X. Z. Yue, *Adv. Sci.* **2022**, *9*, 2201773.

[28] Y. Li, Q. Zhao, Y. Zhang, Y. Li, L. Fan, F.-T. Li, X. Li, *Appl. Catal., B* **2022**, *300*, 120763.

[29] Q. Chen, S. Wu, Y. Xin, *Chem. Eng. J.* **2016**, *302*, 377.

[30] J. Ma, X. Liu, R. Wang, F. Zhang, G. Tu, *Nano Res.* **2022**, *15*, 5671.

[31] R. Xiao, C. Zhao, Z. Zou, Z. Chen, L. Tian, H. Xu, H. Tang, Q. Liu, Z. Lin, X. Yang, *Appl. Catal., B* **2020**, *268*, 118382.

[32] T. Hou, N. Luo, Y. T. Cui, J. Lu, L. Li, K. E. MacArthur, M. Heggen, R. Chen, F. Fan, W. Tian, S. Jin, F. Wang, *Appl. Catal., B* **2019**, *245*, 262.

[33] S. Wang, B. Y. Guan, X. W. D. Lou, *J. Am. Chem. Soc.* **2018**, *140*, 5037.

[34] M. Q. Yang, Y. J. Xu, W. Lu, K. Zeng, H. Zhu, Q. H. Xu, G. W. Ho, *Nat. Commun.* **2017**, *8*, 14224.

[35] K. M. Cho, K. H. Kim, K. Park, C. Kim, S. Kim, A. Al-Saggaf, I. Gereige, H.-T. Jung, *ACS Catal.* **2017**, *7*, 7064.

[36] S. Yin, J. Li, L. Sun, X. Li, D. Shen, X. Song, P. Huo, H. Wang, Y. Yan, *Inorg. Chem.* **2019**, *58*, 15590.

[37] R. M. Bullock, J. G. Chen, L. Gagliardi, P. J. Chirik, O. K. Farha, C. H. Hendon, C. W. Jones, J. A. Keith, J. Klosin, S. D. Minteer, R. H. Morris, A. T. Radosevich, T. B. Rauchfuss, N. A. Strotman, A. Vojvodic, T. R. Ward, J. Y. Yang, Y. Surendranath, *Science* **2020**, *369*, eabc3183.

[38] a) S.-L. Li, K. Tsukagoshi, E. Orgiu, P. Samorì, *Chem. Soc. Rev.* **2016**, *45*, 118; b) C. Kim, I. Moon, D. Lee, M. S. Choi, F. Ahmed, S. Nam, Y. Cho, H.-J. Shin, S. Park, W. J. Yoo, *ACS Nano* **2017**, *11*, 1588.

[39] W. Zhou, X. Zou, S. Najmaei, Z. Liu, Y. Shi, J. Kong, J. Lou, P. M. Ajayan, B. I. Yakobson, J.-C. Idrobo, *Nano Lett.* **2013**, *13*, 2615.

[40] K. Zhang, J. K. Kim, B. Park, S. Qian, B. Jin, X. Sheng, H. Zeng, H. Shin, S. H. Oh, C.-L. Lee, J. H. Park, *Nano Lett.* **2017**, *17*, 6676.

[41] X. Wang, X. Wang, J. Huang, S. Li, A. Meng, Z. Li, *Nat. Commun.* **2021**, *12*, 4112.

[42] S. Zhang, X. Liu, C. Liu, S. Luo, L. Wang, T. Cai, Y. Zeng, J. Yuan, W. Dong, Y. Pei, Y. Liu, *ACS Nano* **2018**, *12*, 751.

[43] M. Zhao, F. Huang, H. Lin, J. Zhou, J. Xu, Q. Wu, Y. Wang, *Nanoscale* **2016**, *8*, 16670.

[44] L. Du, Y. Chen, Q. Wang, Y. Zhao, L. Li, X. Liu, G. Tian, *Small* **2021**, *17*, 2100412.

[45] J. Yang, X. Zhu, Z. Mo, J. Yi, J. Yan, J. Deng, Y. Xu, Y. She, J. Qian, H. Xu, H. Li, *Inorg. Chem. Front.* **2018**, *5*, 3163.

[46] J. Zhang, B. D. Chernomordik, R. W. Crisp, D. M. Kroupa, J. M. Luther, E. M. Miller, J. Gao, M. C. Beard, *ACS Nano* **2015**, *9*, 7151.

[47] J. Ji, X. Song, J. Liu, Z. Yan, C. Huo, S. Zhang, M. Su, L. Liao, W. Wang, Z. Ni, Y. Hao, H. Zeng, *Nat. Commun.* **2016**, *7*, 13352.

[48] H. Ago, S. Fukamachi, H. Endo, P. Solís-Fernández, R. Mohamad Yunus, Y. Uchida, V. Panchal, O. Kazakova, M. Tsuji, *ACS Nano* **2016**, *10*, 3233.

[49] A. Prudnikau, A. Chuvilin, M. Artemyev, *J. Am. Chem. Soc.* **2013**, *135*, 14476.

[50] B. Ji, Y. E. Panfil, N. Waiskopf, S. Remennik, I. Popov, U. Banin, *Nat. Commun.* **2019**, *10*, 2.

[51] B. M. Wieliczka, A. L. Kaledin, W. E. Buhro, R. A. Loomis, *ACS Nano* **2018**, *12*, 5539.

[52] F. You, J. Wan, J. Qi, D. Mao, N. Yang, Q. Zhang, L. Gu, D. Wang, *Angew. Chem. Int. Ed.* **2020**, *59*, 721.

[53] X. Wang, Z. Wang, J. Zhang, X. Wang, Z. Zhang, J. Wang, Z. Zhu, Z. Li, Y. Liu, X. Hu, J. Qiu, G. Hu, B. Chen, N. Wang, Q. He, J. Chen, J. Yan, W. Zhang, T. Hasan, S. Li, H. Li, H. Zhang, Q. Wang, X. Huang, W. Huang, *Nat. Commun.* **2018**, *9*, 3611.

[54] D. Aldakov, A. Lefrançois, P. Reiss, *J. Mater. Chem. C* **2013**, *1*, 3756.

[55] S. Chen, D. Huang, M. Cheng, L. Lei, Y. Chen, C. Zhou, R. Deng, B. Li, *J. Mater. Chem. A* **2021**, *9*, 196.

[56] a) A. Agrawal, S. H. Cho, O. Zandi, S. Ghosh, R. W. Johns, D. J. Milliron, *Chem. Rev.* **2018**, *118*, 3121; b) Y. Xie, L. Carbone, C. Nobile, V. Grillo, S. D'Agostino, F. Della Sala, C. Giannini, D. Altamura, C. Oelsner, C. Kryschi, P. D. Cozzoli, *ACS Nano* **2013**, *7*, 7352.

[57] a) C. Coughlan, M. Ibáñez, O. Dobrozhan, A. Singh, A. Cabot, K. M. Ryan, *Chem. Rev.* **2017**, *117*, 5865; b) T. M. Mattox, X. Ye, K. Manthiram, P. J. Schuck, A. P. Alivisatos, J. J. Urban, *Adv. Mater.* **2015**, *27*, 5830; c) A. Comin, L. Manna, *Chem. Soc. Rev.* **2014**, *43*, 3957.

[58] a) X. Wang, Z. Miao, Y. Ma, H. Chen, H. Qian, Z. Zha, *Nanoscale* **2017**, *9*, 14512; b) Q. Bai, M. Liang, W. Wu, C. Zhang, X. Li, M. Liu, D. Yang, W. W. Yu, Q. Hu, L. Wang, F. Du, N. Sui, Z. Zhu, *Adv. Funct. Mater.* **2022**, *32*, 2112683.

[59] a) D. Hong, W. Zang, X. Guo, Y. Fu, H. He, J. Sun, L. Xing, B. Liu, X. Xue, *ACS Appl. Mater. Interfaces* **2016**, *8*, 21302; b) S. K. Han, C. Gu, S. Zhao, S. Xu, M. Gong, Z. Li, S. H. Yu, *J. Am. Chem. Soc.* **2016**, *138*, 12913.

[60] J. Cui, Y. Li, L. Liu, L. Chen, J. Xu, J. Ma, G. Fang, E. Zhu, H. Wu, L. Zhao, L. Wang, Y. Huang, *Nano Lett.* **2015**, *15*, 6295.

[61] a) C. Gong, L. Colombo, R. M. Wallace, K. Cho, *Nano Lett.* **2014**, *14*, 1714; b) H. Huang, Z. Tan, Y. He, J. Liu, J. Sun, K. Zhao, Z. Zhou, G. Tian, S. L. Wong, A. T. Wee, *ACS Nano* **2016**, *10*, 3198.

[62] Y. Ma, X. Wang, Y. Jia, X. Chen, H. Han, C. Li, *Chem. Rev.* **2014**, *114*, 9987.

[63] H. Li, W. Tu, Y. Zhou, Z. Zou, *Adv. Sci.* **2016**, *3*, 1500389.

[64] Y. Liu, J. Sun, X. Zhou, C. Lv, Y. Zhou, B. Cong, G. Chen, *Chem. Eng. J.* **2022**, *437*, 135280.

[65] Z. Li, J. Hou, B. Zhang, S. Cao, Y. Wu, Z. Gao, X. Nie, L. Sun, *Nano Energy* **2019**, *59*, 537.

[66] R. Das, R. Paul, A. Parui, A. Shrotri, C. Atzori, K. A. Lomachenko, A. K. Singh, J. Mondal, S. C. Peter, *J. Am. Chem. Soc.* **2023**, *145*, 422.

[67] C. Xue, H. An, X. Yan, J. Li, B. Yang, J. Wei, G. Yang, *Nano Energy* **2017**, *39*, 513.

[68] Y. J. Yuan, D. Chen, J. Zhong, L. X. Yang, J. Wang, M. J. Liu, W. G. Tu, Z. T. Yu, Z. G. Zou, *J. Mater. Chem. A* **2017**, *5*, 15771.

[69] W. Y. Lim, H. Wu, Y. F. Lim, G. W. Ho, *J. Mater. Chem. A* **2018**, *6*, 11416.

[70] J. Wu, Z. Zhang, Y. Fang, K. Liu, J. Huang, Q. Yuan, B. Dong, *Chem. Eng. J.* **2022**, *437*, 135308.

[71] a) M. R. Shcherbakov, H. Zhang, M. Tripepi, G. Sartorello, N. Talisa, A. AlShafey, Z. Fan, J. Twardowski, L. A. Krivitsky, A. I. Kuznetsov, E. Chowdhury, G. Shvets, *Nat. Commun.* **2021**, *12*, 4185; b) Z. Liu, Y. Liu, P. Xu, Z. Ma, J. Wang, H. Yuan, *ACS Appl. Mater. Interfaces* **2017**, *9*, 20620; c) Q. Zhang, Y. Huang, L. Xu, J. J. Cao, W. Ho, S. C. Lee, *ACS Appl. Mater. Interfaces* **2016**, *8*, 4165.

[72] J. J. Velázquez-Salazar, L. Bazán-Díaz, Q. Zhang, R. Mendoza-Cruz, L. Montaño-Priede, G. Guisbiers, N. Large, S. Link, M. José-Yacamán, *ACS Nano* **2019**, *13*, 10113.

[73] a) P. S. Shinde, S. Y. Lee, S. H. Choi, H. H. Lee, J. Ryu, J. S. Jang, *Sci. Rep.* **2016**, *6*, 32436; b) Z. Lian, M. Sakamoto, J. J. M. Vequizo, C. S. K. Ranasinghe, A. Yamakata, T. Nagai, K. Kimoto, Y. Kobayashi, N. Tamai, T. Teranishi, *J. Am. Chem. Soc.* **2019**, *141*, 2446; c) Z. Luo, X. Ye, S. Zhang, S. Xue, C. Yang, Y. Hou, W. Xing, R. Yu, J. Sun, Z. Yu, X. Wang, *Nat. Commun.* **2022**, *13*, 2230; d) L. Ju, Y. Dai, W. Wei, M. Li, Y. Liang, B. Huang, *Phys. Chem. Chem. Phys.* **2018**, *20*, 1904.

[74] Z. Ren, X. Liu, H. Chu, H. Yu, Y. Xu, W. Zheng, W. Lei, P. Chen, J. Li, C. Li, *J. Colloid Interface Sci.* **2017**, *488*, 190.

[75] a) R. Alam, M. Labine, C. J. Karwacki, P. V. Kamat, *ACS Nano* **2016**, *10*, 2880; b) Z. Lian, M. Sakamoto, H. Matsunaga, J. J. M. Vequizo, A. Yamakata, M. Haruta, H. Kurata, W. Ota, T. Sato, T. Teranishi, *Nat. Commun.* **2018**, *9*, 2314.

[76] a) Q. Zhang, A. Mirzaei, Y. Wang, G. Song, C. Wang, L. V. Besteiro, A. O. Govorov, M. Chaker, D. Ma, *Appl. Catal., B* **2022**, *317*, 121792; b) L. Wang, Z. Chen, G. Liang, Y. Li, R. Lai, T. Ding, K. Wu, *Nat. Commun.* **2019**, *10*, 4532.

[77] Q. Zhang, J. Deng, Z. Xu, M. Chaker, D. Ma, *ACS Catal.* **2017**, *7*, 6225.

[78] J. Li, S. K. Cushing, J. Bright, F. Meng, T. R. Senty, P. Zheng, A. D. Bristow, N. Wu, *ACS Catal.* **2013**, *3*, 47.

[79] S. Wu, H. Pang, W. Zhou, B. Yang, X. Meng, X. Qiu, G. Chen, L. Zhang, S. Wang, X. Liu, R. Ma, J. Ye, N. Zhang, *Nanoscale* **2020**, *12*, 8693.

[80] K. Li, Y. Cai, X. Yang, S. Wang, C. Teng, Y. Tian, Q. Min, W. Zhu, *Adv. Funct. Mater.* **2022**, *32*, 2113002.

[81] J. Tao, M. Wang, X. Zhang, L. Lu, H. Tang, Q. Liu, S. Lei, G. Qiao, G. Liu, *Appl. Catal., B* **2023**, *320*, 122004.

[82] M. Ma, J. Liu, H. Zhao, S. Yue, L. Zhong, Y. Huang, X. Jia, K. Liu, X. Li, Z. Wang, S. Qu, Y. Lei, *Appl. Catal., B* **2023**, *325*, 122327.

[83] Q. Guo, F. Liang, X. B. Li, Y. J. Gao, M. Y. Huang, Y. Wang, S. G. Xia, X. Y. Gao, Q. C. Gan, Z. S. Lin, C. H. Tung, L. Z. Wu, *Chem* **2019**, *5*, 2605.

[84] J. Zou, G. Liao, H. Wang, Y. Ding, P. Wu, J. P. Hsu, J. Jiang, *J. Alloys Compd.* **2022**, *911*, 165020.

[85] Q. Gao, L. Zhou, S. Xu, S. Dai, Q. Zhu, Y. Li, *Environ. Sci. Nano* **2023**, *10*, 581.

[86] a) L. Zhou, S. Dai, S. Xu, Y. She, Y. Li, S. Leveneur, Y. Qin, *Appl. Catal., B* **2021**, *291*, 120019; b) Q. Chen, H. Zhou, J. Wang, J. Bi, F. Dong, *Appl. Catal., B* **2022**, *307*, 121182; c) Z. Kang, Q. Liu, X. Zhang, X. Zhang, D. P. Yang, X. Chen, *Chemosphere* **2022**, *307*, 135789.

[87] G. Liu, A. W. Robertson, M. M. J. Li, W. C. H. Kuo, M. T. Darby, M. H. Muhieddine, Y. C. Lin, K. Suenaga, M. Stamatakis, J. H. Warner, S. C. E. Tsang, *Nat. Chem.* **2017**, *9*, 810.

[88] D. Ryaboshapka, L. Piccolo, M. Aouine, P. Bargiela, V. Briois, P. Afanasiev, *Appl. Catal., B* **2022**, *302*, 120831.

[89] L. Ju, X. Tan, X. Mao, Y. Gu, S. Smith, A. Du, Z. Chen, C. Chen, L. Kou, *Nat. Commun.* **2021**, *12*, 5128.

[90] H. Liu, D. Grasseschi, A. Dodda, K. Fujisawa, D. Olson, E. Kahn, F. Zhang, T. Zhang, Y. Lei, R. B. N. Branco, A. L. Elías, R. C. Silva, Y. T. Yeh, C. M. Maroneze, L. Seixas, P. Hopkins, S. Das, C. J. S. de Matos, M. Terrones, *Sci. Adv.* **2020**, *6*, eabc9308.

[91] J. Zhang, X. Xu, L. Yang, D. Cheng, D. Cao, *Small Methods* **2019**, *3*, 1900653.

[92] F. Niu, W. Tu, X. Lu, H. Chi, H. Zhu, X. Zhu, L. Wang, Y. Xiong, Y. Yao, Y. Zhou, Z. Zou, *ACS Catal.* **2022**, *12*, 4481.

[93] a) S. Anantharaj, S. R. Ede, K. Sakthikumar, K. Karthick, S. Mishra, S. Kundu, *ACS Catal.* **2016**, *6*, 8069; b) F. Zhang, H. Q. Zhuang, J. Song, Y. L. Men, Y. X. Pan, S. H. Yu, *Appl. Catal., B* **2018**, *226*, 103.

[94] D. Zeng, L. Xiao, W. J. Ong, P. Wu, H. Zheng, Y. Chen, D. L. Peng, *ChemSusChem* **2017**, *10*, 4624.

[95] C. Bie, B. Zhu, L. Wang, H. Yu, C. Jiang, T. Chen, J. Yu, *Angew. Chem. Int. Ed.* **2022**, *61*, 202212045.

[96] Y. L. Li, Q. Zhao, S. J. Liu, G. Ma, Y. Liu, R. H. Liu, H. Y. Mu, X. Li, F. T. Li, *Chem. Eng. J.* **2022**, *446*, 137399.

[97] J. Ran, H. Zhang, S. Fu, M. Jaroniec, J. Shan, B. Xia, Y. Qu, J. Qu, S. Chen, L. Song, J. M. Cairney, L. Jing, S. Z. Qiao, *Nat. Commun.* **2022**, *13*, 4600.

[98] Y. Wang, J. Zhao, W. Hou, Y. Xu, *Appl. Catal., B* **2022**, *310*, 121350.

[99] W. Liu, P. Wang, Y. Ao, J. Chen, X. Gao, B. Jia, T. Ma, *Adv. Mater.* **2022**, *34*, 2202508.

[100] F. Zhang, H.-Q. Zhuang, W. Zhang, J. Yin, F. H. Cao, Y. X. Pan, *Catal. Today* **2019**, *330*, 203.

[101] X. Sang, Y. Xie, M. W. Lin, M. Alhabeb, K. L. Van Aken, Y. Gogotsi, P. R. C. Kent, K. Xiao, R. R. Unocic, *ACS Nano* **2016**, *10*, 9193.

[102] H. Li, Y. Tan, P. Liu, C. Guo, M. Luo, J. Han, T. Lin, F. Huang, M. Chen, *Adv. Mater.* **2016**, *28*, 8945.

[103] G. Ye, Y. Gong, J. Lin, B. Li, Y. He, S. T. Pantelides, W. Zhou, R. Vajtai, P. M. Ajayan, *Nano Lett.* **2016**, *16*, 1097.

[104] J. Li, X. Wu, W. Pan, G. Zhang, H. Chen, *Angew. Chem. Int. Ed.* **2018**, *57*, 491.

[105] Y. Pan, Y. Chen, K. Wu, Z. Chen, S. Liu, X. Cao, W. C. Cheong, T. Meng, J. Luo, L. Zheng, C. Liu, D. Wang, Q. Peng, J. Li, C. Chen, *Nat. Commun.* **2019**, *10*, 4290.

[106] R. Chen, Z. Ren, Y. Liang, G. Zhang, T. Dittrich, R. Liu, Y. Liu, Y. Zhao, S. Pang, H. An, C. Ni, P. Zhou, K. Han, F. Fan, C. Li, *Nature* **2022**, *610*, 296.

[107] a) S. Wang, Y. Gao, S. Miao, T. Liu, L. Mu, R. Li, F. Fan, C. Li, *J. Am. Chem. Soc.* **2017**, *139*, 11771; b) Q. Zhang, H. Li, L. Gan, Y. Ma, D. Golberg, T. Zhai, *Chem. Soc. Rev.* **2016**, *45*, 2694.

[108] Q. Chen, Y. Liu, X. Gu, D. Li, D. Zhang, D. Zhang, H. Huang, B. Mao, Z. Kang, W. Shi, *Appl. Catal., B* **2022**, *301*, 120755.

[109] W. Wang, Y. Tao, J. Fan, Z. Yan, H. Shang, D. L. Phillips, M. Chen, G. Li, *Adv. Funct. Mater.* **2022**, *32*, 2201357.

[110] Y. Xin, S. Li, Y. Qian, W. Zhu, H. Yuan, P. Jiang, R. Guo, L. Wang, *ACS Catal.* **2020**, *10*, 11280.

[111] L. J. Chen, T. T. Liu, S. M. Liu, S. Cai, X. X. Zou, J. W. Jiang, Z. Y. Mei, G. F. Zhao, X. Yang, H. Guo, *Rare Met.* **2022**, *41*, 144.

[112] Z. Zhao, Z. Liu, Z. Zhu, F. Wang, F. Teng, W. Jiang, Y. Yang, *Chin. Chem. Lett.* **2021**, *32*, 2474.

[113] T. Di, B. Zhu, B. Cheng, J. Yu, J. Xu, *J. Catal.* **2017**, *352*, 532.

[114] J. Gan, H. Wang, H. Hu, M. Su, F. Chen, H. Xu, *Appl. Surf. Sci.* **2021**, *564*, 150396.

[115] Y. Zhang, Y. Wu, L. Wan, H. Ding, H. Li, X. Wang, W. Zhang, *Appl. Catal., B* **2022**, *311*, 121255.

[116] J. Lu, Z. Zhang, L. Cheng, H. Liu, *New J. Chem.* **2020**, *44*, 13728.

[117] J. Xu, W. Zhong, D. Gao, X. Wang, P. Wang, H. Yu, *Chem. Eng. J.* **2022**, *439*, 135758.

[118] Y. Yang, B. Cheng, J. Yu, L. Wang, W. Ho, *Nano Res.* **2021**, https://doi.org/10.1007/s12274-021-3733-0.

[119] Y. Yang, Z. Wu, R. Yang, Y. Li, X. Liu, L. Zhang, B. Yu, *Appl. Surf. Sci.* **2021**, *539*, 148220.

[120] T. Xie, Y. Liu, H. Wang, Z. Wu, *Appl. Surf. Sci.* **2018**, *444*, 320.

Mengmeng Ma received her B.S. degree from Beijing University of Science and Technology in 2019. Now she is a Ph.D. student at the Institute of Semiconductors, Chinese Academy of Science, under the supervision of Professor Zhijie Wang and Shengchun Qu. Her current work focuses on nanomaterials and technology for photo(electro)chemistry.

Huaping Zhao obtained his Ph.D. in materials science from the State Key Laboratory of Crystal Materials of Shandong University in 2007. Following two years of postdoctoral research at the Institute of Chemistry (Chinese Academy of Sciences, 2007–2009), he was employed as a scientist by the University of Muenster from 2009 to 2011. Since 2012, he has been a senior scientist (permanent) in Prof. Yong Lei's group at the Technical University of Ilmenau, Germany. His current research focus is the design and fabrication of functional nanostructures for energy storage and conversion.

Zhijie Wang received his B.S. degree in 2004 from Zhejiang University and his Ph.D. degree in 2009 from the Institute of Semiconductors, Chinese Academy of Sciences. After 4 years of postdoc research at the University of Wyoming and the University of Michigan, he worked as a senior scientist and a junior group leader at the Ilmenau University of Technology (Germany) in the 3D Nanostructuring Group of Prof. Yong Lei since 2013. He is currently a professor at the Institute of Semiconductors, Chinese Academy of Sciences. His research interest includes nanomaterials, nano-devices, energy-related sciences, surface science, and photoelectrochemistry.

Yong Lei is a professor and head of group (Chair) of applied nano-physics at the Technical University of Ilmenau, Germany. He began working in Germany in 2003 as an Alexander von Humboldt Fellow at the Karlsruhe Institute of Technology. From 2006, he was a group leader at the University of Muenster and a junior professor. In 2011, he joined the Technical University of Ilmenau as a professor. His research focus is on template-based nanostructuring, energy conversion and storage devices, and optoelectronic applications of functional nanostructures. He has received prestigious European and German funding awards, such as two European Research Council Grants.